From the subtropics to the central equatorial Pacific Ocean: neodymium isotopic composition and rare earth element concentration variations

Mélanie Grenier, C. Jeandel, F. Lacan, D. Vance, C. Venchiarutti, A. Cros, Sophie Cravatte

JOURNAL OF GEOPHYSICAL RESEARCH: OCEANS, VOL. 118, 592–618, doi:10.1029/2012JC008239, 2013

From the subtropics to the central equatorial Pacific Ocean: Neodymium isotopic composition and rare earth element concentration variations

Mélanie Grenier,[1] Catherine Jeandel,[1] François Lacan,[1] Derek Vance,[2] Célia Venchiarutti,[1,3] Alexandre Cros,[1,4] and Sophie Cravatte[1,5]

Received 31 May 2012; revised 15 November 2012; accepted 18 November 2012; published 4 February 2013.

[1] Neodymium isotopic compositions (ε_{Nd}) and rare earth element (REE) concentrations were measured for filtered surface to deep waters (112 samples) in the Southern Tropical Pacific. The relatively detailed picture of these tracer distributions allowed us to refine the areas where oceanic ε_{Nd} variations occur. ε_{Nd} values increase for most of the water masses flowing from Samoa to the Solomon Sea and in the Papua New Guinea (PNG) area, as already observed. Furthermore, water masses arriving from the eastern equatorial Pacific (200–550 m depth) also revealed radiogenic values, possibly acquired in the vicinity of the South American coasts and Galapagos Islands. These ε_{Nd} variations affect the whole water column. The most likely process causing such variations is "boundary exchange" between the numerous radiogenic slopes/margins located in this area and seawater flowing past. Dissolution of atmospheric deposition and/or diffuse streaming of volcanic ash are also suggested to explain the radiogenic ε_{Nd} observed at the surface in the PNG area. Interestingly, a positive europium (Eu) anomaly characterizes the normalized REE patterns of most of the studied water masses. This anomaly is consistent with the REE patterns of sediment and rock samples that are potential sources for the local waters. Such consistency reinforces the hypothesis that lithogenic sources play a major role in the oceanic REE budget, thanks to "boundary exchange." The data set presented here is a good basis for further sampling that will be realized in the framework of the ongoing GEOTRACES program (www.geotraces.org).

Citation: Grenier, M., C. Jeandel, F. Lacan, D. Vance, C. Venchiarutti, A. Cros, and S. Cravatte (2013), From the subtropics to the central equatorial Pacific Ocean: Neodymium isotopic composition and rare earth element concentration variations, *J. Geophys. Res. Oceans*, *118*, 592–618, doi:10.1029/2012JC008239.

1. Introduction

[2] Dissolved chemical elements in seawater, particularly those associated with isotopic tracers, allow better understanding of water mass histories and clarify the sources of key nutrient species to the oceans [e.g., *Lacan and Jeandel*, 2001], with implications for the impact of oceanic productivity on the global carbon cycle. Between 100 m and about 1000 m depth, the equatorial Pacific circulation is fed by a redistribution of waters from the large open ocean subtropical gyres toward the equator, mainly via the low-latitude western boundary currents [*Fine et al.*, 1994; *Bostock et al.*, 2010; *Grenier et al.*, 2011]. Upwelling of these waters in the equatorial Pacific controls nutrient and micronutrient supply to the surface ocean, modulating primary production in the high-nutrient, low-chlorophyll (HNLC) area [*Coale et al.*, 1996; *Ryan et al.*, 2006; *Slemons et al.*, 2009], and helping to set the concentration of carbon dioxide in the atmosphere. Several studies have concluded that the western coastal area of the equatorial Pacific, in particular the Papua New Guinea (PNG) coast, is a major source of some elements for the water masses flowing past it, including important micronutrients like Fe [*Johnson and McPhaden*, 1999; *Lacan and Jeandel*, 2001; *Mackey et al.*, 2002; *Slemons et al.*, 2010]. Owing to the major role of the strong western boundary currents feeding the Equatorial Undercurrent (EUC) in transporting limiting nutrients as far as the eastern equatorial Pacific, understanding the processes that control this source is of prime importance.

[3] The isotopic composition of the rare earth element (REE) Nd is a very powerful tracer that allows the

[1]Laboratoire d'Etudes en Géophysique et Océanographie Spatiales (LEGOS), Université de Toulouse, CNRS (Centre National de Recherche Scientifique), CNES (Centre National d'Etudes Spatiales), IRD (Institut de Recherche pour le Développement), Toulouse, France.
[2]Department of Earth Sciences, Bristol Isotope Group, University of Bristol, Bristol, UK.
[3]Now at Institute for Reference Materials and Measurements (IRMM), Joint Research Centre (JRC), Geel, Belgium.
[4]Now at Laboratoire Intéractions et Dynamique des Environnements de Surface (IDES), Université Paris Sud, Orsay, France.
[5]LEGOS, IRD, Université de Toulouse, CNRS, CNES, Nouméa, New Caledonia.

Corresponding author: M. Grenier, LEGOS, 14 Avenue Edouard Belin, F-31400 Toulouse, France. (melanie.grenier@legos.obs-mip.fr)

2169-9275/13/10.1029/2012JC008239

characterization of the sources of lithogenic elements to the ocean. One of the seven Nd isotopes, ^{143}Nd, is formed by α-decay of ^{147}Sm. Consequently, its natural abundance varies and depends on the time-integrated Sm/Nd ratio of the rock from which the Nd is derived. This variation is expressed as ε_{Nd}:

$$\varepsilon_{Nd} = \left(\frac{\left(^{143}Nd/^{144}Nd\right)_{sample}}{\left(^{143}Nd/^{144}Nd\right)_{CHUR}} - 1 \right) * 10^4$$

where CHUR stands for chondritic uniform reservoir and represents an average Earth value, presently 0.512638 [*Wasserburg et al*., 1981].

[4] Igneous rocks recently extracted from the Earth's mantle have more radiogenic ε_{Nd} values, greater than zero, whereas less radiogenic ε_{Nd} values, lower than −10, characterize old continental crust. The heterogeneity of the ε_{Nd} signatures of the rocks outcropping around the ocean margins is nicely represented in *Jeandel et al*. [2007]. In the ocean, ε_{Nd} signatures of the different waters conveyed by the thermohaline circulation increase from approximately −15 in the North Atlantic to −4 in the North Pacific, whereas the concentrations only double [*Lacan et al*., 2012]. This relatively small increase of the deep Nd concentrations is far less than that which would result from the Nd flux required to change the ε_{Nd} values. This apparent contradiction has been called the Nd paradox [*Bertram and Elderfield*, 1993; *Jeandel et al*., 1995; *Goldstein and Hemming*, 2003]. In addition, the change in the ε_{Nd} values requires Nd inputs characterized by very radiogenic values in the Pacific, more radiogenic than both the atmospheric dust and dissolved riverine flux delivered to the Pacific. Solving the paradox therefore requires (i) significant fluxes of Nd characterized by radiogenic values around the Pacific and non-radiogenic sources in the Atlantic; (ii) scavenging of a large fraction of the added Nd, in order to maintain a relatively constant concentration, while achieving the modification of the isotope ratio and (iii) dissolved/particulate exchange throughout the water column, consistent with this scavenging and the Si-like vertical profile of Nd [*Tachikawa et al*., 2003]. These different constraints concerning the oceanic Nd budget led *Lacan and Jeandel* [2005] to introduce the concept of "boundary exchange", a mechanism coupling the release of dissolved Nd from sediment deposited on the ocean margins to the dissolved pool with the removal of dissolved chemical elements from seawater toward the sediments, later modeled by *Arsouze et al*. [2009]. In the equatorial Pacific, *Lacan and Jeandel* [2001] used the variations in neodymium (Nd) isotopic signature along 140°W to argue for a release of Nd from dissolution of PNG margin sediments.

[5] In parallel, processes governing the oceanic REE distribution have been investigated in many studies for 30 years. Most of these studies conclude that internal processes occurring within the water column control the characteristic pattern of oceanic REE concentrations [*De Baar et al*., 1985; *Byrne and Kim*, 1990, 1993; *Lee and Byrne*, 1993; *Tachikawa et al*., 1999; *Takebe*, 2005; *Akagi et al*., 2011]. However, several authors have also proposed that the shape of REE patterns could be significantly impacted by the release of dissolved REE to the open ocean from river discharge and remineralization of margin sediments [*Sholkovitz et al*., 1994; *Amakawa et al*., 2000; *Nozaki and Alibo*, 2003a, 2003b; *Wang and Yamada*, 2007].

[6] This study will specifically address the following questions: Where do the ε_{Nd} and REE parameter changes of water masses occur? What are the processes that likely govern these variations? What information do geochemical and hydrological properties bring to bear on water mass pathways and mixing?

[7] This work characterizes ε_{Nd} and REE concentrations of surface, intermediate and deep-filtered waters from 17 stations (112 samples), between the Coral Sea and 140°W-0°. The geochemical data are supported by the availability of a detailed hydrological context, giving us essential backup information on water mass pathways. Furthermore, ε_{Nd} and REE concentration measurements are paired with data on salinity and oxygen, allowing rigorous interpretation of the geochemical measurements as a function of known water mass pathways. The new data also allow us to suggest some new details to already known features. The REE concentration distributions were investigated by comparing the REE patterns and their vertical profiles to data for solid material (rocks and sediments) published in the literature.

[8] Section 2 describes the sampling and the analytical procedure in this study. The hydrological context of the studied area is presented in section 3. Section 4 presents the geochemical results. We discuss the results in section 5 and conclude in section 6.

2. Materials and Methods

[9] Most of the seawater samples were collected during the EUC-Fe cruise (R/V Kilo Moana, PI J. Murray) in August–September 2006. Two stations were also sampled during the FLUSEC-01 cruise [*Maes et al*., 2009; *Gasparin et al*., 2012] in August 2007, allowing the collection of samples in the Coral Sea, north of New Caledonia (station FLUSEC 43) and in the Solomon Sea (station FLUSEC 22). The sampling locations are plotted in Figure 1. The EUC-Fe stations are located along a section starting in the central Pacific and ending close to the Papua New Guinea coast, between 140°W and 143°E and covering the latitude range 2°N-6°S. Conductivity, temperature, depth (CTD) and oxygen measurements were also carried out at all the stations occupied during this cruise. Acoustic Doppler current profiler (ADCP) data and other samples for chemical analyses were also acquired during the cruise for the characterization of seawater content in trace metals, nutrients and aerosols and are detailed online (http://www.ocean.washington.edu/cruises/KiloMoana2006/).

[10] Surface, subsurface and intermediate waters were characterized for most of the stations. Deep and bottom water samples were collected along the Papua New Guinea coast, along the New Ireland coast, and at 180°E-0°N (stations 29, 28, 24, and 14 in Figure 1).

[11] Note that ε_{Nd} and REE concentrations of sediments originating from the Bismarck Sea, upstream and in front of the Sepik River (kindly provided by J. Murray), and of volcanic ash samples from New Britain (collected by F. Lacan) were analyzed by the Service d'Analyse des Roches et des Minéraux (http://www.crpg.cnrs-nancy.fr/SARM/). The analytical protocols for these latter analyses of solid materials are described in *Carignan et al*. [2001] and we do not detail them here.

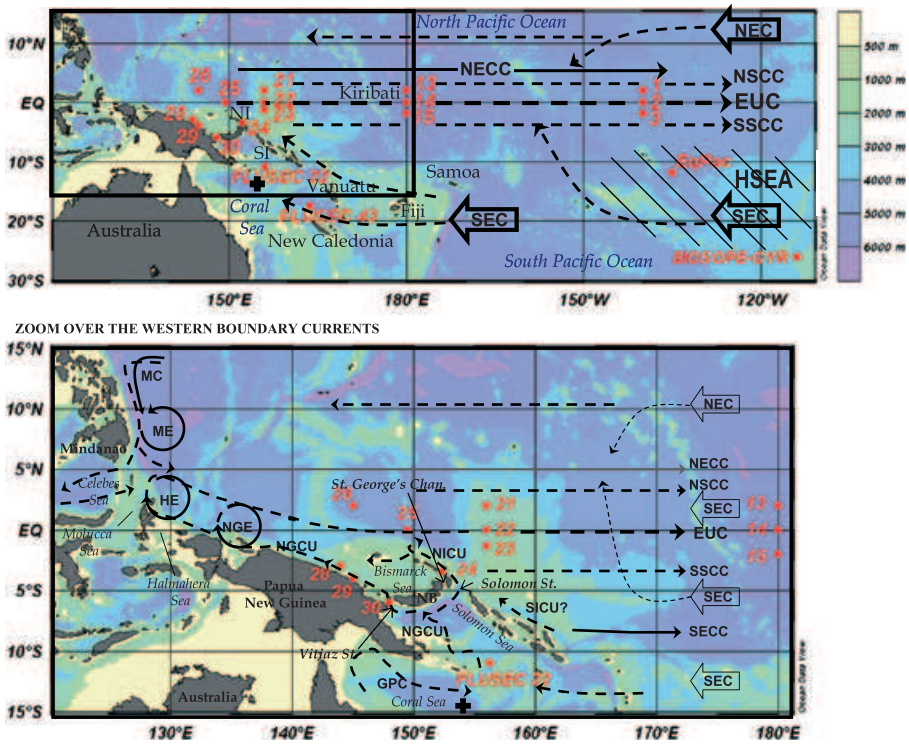

Figure 1. Sample location map. The bottom panel zooms in on the western boundary area, indicated on the top panel by a black rectangle. The sampling locations are represented by red circles. Number-associated stations correspond to EUC-Fe cruise. The two stations sampled in the Coral and Solomon Seas correspond to FLUSEC-01 cruise. "EqPac" and "BIOSOPE-GYR," respectively, studied by *Lacan and Jeandel* [2001] and *Jeandel et al*. [2013], are also identified. The major surface currents (solid arrows) and subsurface currents (dashed arrows) are shown in the equatorial/tropical Pacific Ocean [*Grenier et al*., 2011]: westward North Equatorial Current (NEC) and South Equatorial Current (SEC); equatorward Mindanao Current (MC), New Guinea Coastal Undercurrent (NGCU), New Ireland Coastal Undercurrent (NICU) and Solomon Island Coastal Undercurrent (SICU); eastward Gulf of Papua Current (GPC), North and South Subsurface Countercurrents (NSCC and SSCC, respectively) also called Tsuchiya Jets, North and South Equatorial Countercurrents (NECC and SECC, respectively), and Equatorial Undercurrent (EUC). The main islands are identified, among which New Ireland (NI), Solomon Islands (SI), and New Britain (NB). The Mindanao Eddy (ME), the Halmahera Eddy (HE) and the New Guinea Eddy (NGE) are also shown. Vitiaz and Solomon Straits and St. George's Channel are identified. The black cross refers to the SA-7 station we used as a reference for our REE concentrations [*Zhang and Nozaki*, 1996]. The high evaporation surface area (HSEA) is hatched.

2.1. Nd Isotopic Composition

[12] For Nd isotope measurements, 12 L Niskin bottles mounted on a CTD rosette were used. Two bottles were triggered at the same depth to collect a 20 L sample. The 20 L of seawater was filtered onboard through 0.4 μm pore size, 47 mm diameter Nuclepore membranes in the built-in clean room of the vessel. Filtered samples were transferred into pre-cleaned 20 L plastic cubic containers and then acidified to pH = 2 with 15 mL of Suprapur HCl 30%. At this juncture, 0.5 L aliquots were stored for the REE measurements. Most of the samples presented in this study were pre-concentrated onboard shortly after the sampling. For this purpose, their pH was increased to 3.4–3.7 by adding NH_4OH. Each 20 L sample was pre-concentrated using four C18 SepPak cartridges loaded with a REE complexant (HDEHP/H_2MEHP) [*Shabani et al*., 1992]. Back at the land-based laboratory, the REEs were eluted using 6 *M* HCl, dried and then dissolved again in 1.5 mL of 1 *M* HCl. This solution was loaded on a cation exchange column (0.6 cm in diameter, 4.8 cm in height) packed with Biorad AG50W-X8 200–400 mesh resin and rinsed first with HCl and then HNO_3 in order to extract the remaining matrix while retaining the REE on the column. The REEs were then eluted with 6 mL of 6 *M* HCl [*Rickli et al*., 2010]. This solution was dried and dissolved in 0.3 mL of 0.2 *M* HCl for the final extraction of Nd using an anionic exchange column (0.4 cm in diameter, 4 cm in height) packed with 0.5 mL of Ln-Spec resin. A final elution using 2.5 mL of 0.2 *M* HCl permitted recovery of the neodymium. Details of the procedures used on the cationic and anionic columns are described in *Tachikawa et al*. [1999] and *Pin and Zalduegui* [1997], respectively. For Nd isotope analysis of stations EUC-Fe 14, 22, 28, 29, 30, and of the two FLUSEC stations, samples were dissolved again in 1.5 μL of 2 *M* HCl, loaded on a rhenium filament and analyzed isotopically by thermal ionization mass spectrometry (TIMS) in static mode (ThermoFinnigan mass spectrometer MAT 261, Observatoire Midi-Pyrénées, Toulouse). The remaining Nd analysis was performed at the University of Bristol, on a ThermoFinnigan

Neptune multi-collector inductively coupled plasma mass spectrometry (MC-ICP-MS), fitted with nine Faraday collectors with $10^{11}\,\Omega$ resistors and operated with low resolution slits. Both laboratories participated in the GEOTRACES international calibration study [*van de Flierdt et al*., 2012]. For both mass spectrometers, mass fractionation was initially corrected using a $^{146}Nd/^{144}Nd$ ratio of 0.7219. However, as underlined by *Vance and Thirlwall* [2002], MC-ICP-MS generates a residual instrumental mass discrimination that has to be corrected using correlations between $^{146}Nd/^{144}Nd$-normalized $^{143}Nd/^{144}Nd$ and $^{142}Nd/^{144}Nd$. On the TIMS 15 analyses of La Jolla standard were performed to monitor instrumental drift and gave 0.511886 ± 0.000020. The generally accepted value being 0.511860 ± 0.000020, we corrected all the measurements for a machine bias of 0.000026. On the Neptune, 20 analyses of La Jolla standard bracketed multiples of eight samples and gave an average value of 0.511879 ± 0.000005 (2σ). Thus, we corrected all the measurements for a machine bias of 0.000019. Blank contribution to the Nd isotopic measurement was, on average, lower than 1% of the total signal (6 pg).

2.2. Rare Earth Element Concentrations

[13] Rare earth element (REE) concentration measurements were made on aliquots of the same samples as for Nd IC analysis. REEs were extracted from seawater by iron oxide co-precipitation. Each 0.5 L aliquot, first acidified to pH = 2, was spiked with ^{150}Nd (97.84%) and ^{172}Yb (94.9%). Then 680 µL of purified $FeCl_3$ diluted in 0.1 *M* HCl was added. After equilibration, the pH was increased to 7–8 by addition of NH_4OH and co-precipitation took place. The REE-Fe precipitate was extracted by successive centrifugations. It was then dissolved in 1 mL of 6 *M* HCl and loaded on an anion exchange column (0.6 cm in diameter, 7.5 cm in height of the resin bed) packed with 2 mL of AG 1-X8 resin, in order to remove iron. REEs were eluted with 4 mL of 6 *M* HCl. This solution was evaporated and the residue was dissolved again in 0.4 mL of 0.32 *M* HNO_3 for concentration determination using an inductively coupled plasma mass spectrometry (ICP-MS, Agilent 7500). ^{150}Nd and ^{172}Yb spiking allowed us to use isotope dilution to calculate the concentrations of these two REEs. All the REE concentrations have also been determined by external calibration, using indium and rhenium as internal standards to control any sensitivity drift of the machine. Comparing Nd and Yb concentrations deduced from the external calibration to their values deduced from isotope dilution provides the recovery of the whole chemical extraction (average values: 84% and 72% for Nd and Yb, respectively). Corrections for this recovery are then applied linearly to the other REEs [*Lacan and Jeandel*, 2001; *Pahnke et al*., 2012]. Our measurements were characterized by a mass bias error on Nd between 3% and 5% and a precision on Nd concentration of 11%, both with a 95% confidence interval, based on replicates (stations 21 and 23; Table 1). We measured our samples during two ICP-MS sessions. First, REE concentrations of stations GYR, FLUSEC 43, FLUSEC 22, EUC-Fe 30, 29, 28, 22, and 14 were measured. Results of these measurements showed large interferences of BaO with europium 151 (20%), europium 153 (35%), and samarium 152 (20%). For the second measurement session, for the REE measurements of the remaining stations, we coupled a desolvating nebulizer (Aridus II) to the instrument in order to minimize spectral interference and oxide formation [*Chung et al*., 2009; *Pahnke et al*., 2012]. The Aridus caused a decrease in BaO interferences, equal to 0–1% of the Eu signal. The total blank value (averaged on 72 measurements) was lower than 1% of the analyzed REE (III) signal and was 4% for the analyzed Ce signal.

3. Hydrological Context

[14] This section describes the water masses of our study area. The last column of Table 1 summarizes the water mass associated with the collected seawater samples.

3.1. Thermocline Waters

[15] The subsurface circulation patterns presented in Figure 1 are taken from *Grenier et al*. [2011]. No real consensus exists on the nomenclature of thermocline water masses in this region, with different studies using different names that correspond to slightly different water mass properties. Here we adopt the nomenclatures introduced by *Tomczak and Hao* [1989] and *Tsuchiya et al*. [1989]. The salty South Pacific Tropical Waters (SPTW) flow in the upper part of the thermocline ($\sigma_\theta = 24.3$–$25.3\,kg\,m^{-3}$) [*Tsuchiya et al*., 1989] and can be subdivided into two parts. The first branch is the South Pacific Equatorial Water (SPEW) [*Tomczak and Hao*, 1989; *Tsuchiya et al*., 1989; *Tomczak and Godfrey*, 2003], which enters the Coral Sea *north of Vanuatu*. It originates in the subtropical central South Pacific (~20°S) and is formed by subduction of surface water through evaporation in the Polynesian island region. In the following, this formation zone will be referred to as the high surface evaporation area (HSEA; Figure 1). In the Coral Sea, this water is characterized by a high salinity, marked by a peak at $\sim\sigma_\theta = 24.5\,kg\,m^{-3}$ (35.6–35.8) [*Qu and Lindstrom*, 2002] and its relatively high oxygen content ($\sim 140\,\mu mol\,kg^{-1}$; see FLUSEC 22 profiles in Figures 2 and 3). A second branch of SPTW enters the Coral Sea mainly *south of Vanuatu*, conveyed by the North Caledonian Jet (NCJ) [*Gasparin et al*., 2011]. The origins of this thermocline water are not entirely understood, although *Qu and Lindstrom* [2002] suggest subduction in the subtropics around 30°S. In the Coral Sea, this water mass is slightly less saline and more oxygenated than the northern SPEW, and its salinity maximum is centered around $\sigma_\theta = 25.0\,kg\,m^{-3}$ (S = ~35.6 and $O_2 = \sim 160\,\mu mol\,kg^{-1}$; see FLUSEC 43 profiles in Figures 2 and 3) [*Tsuchiya et al*., 1989; *Sokolov and Rintoul*, 2000]. This tropical water (TW) is conveyed eastward by the NCJ to the Australian coast, where part of it bifurcates northward and is conveyed by the Gulf of Papua Current (GPC; Figure 1) before entering the western Solomon Sea. Here, this TW mixes with the SPEW. Then they flow together, within the New Guinea Coastal Undercurrent (NGCU) [*Cravatte et al*., 2011] and reach the equator essentially via the NGCU and the New Ireland Coastal Undercurrent (NICU; Figure 1). A part of the SPEW also flows along the east coasts of the Solomon Islands and New Ireland and reaches the equator north of New Ireland via the NICU.

[16] Upper thermocline waters of northern hemisphere origin reach the equator mostly via the northern Low-Latitude Western Boundary Currents (LLWBCs) [*Tsuchiya et al*., 1989; *Fine et al*., 1994; *Grenier et al*., 2011]. These waters

Table 1. Locations, Depths, Hydrological Properties, Ce Anomalies, Nd Concentrations, Nd ICs and ε_{Nd} of the Samples Analyzed in This Study and the Corresponding Water Masses Identified

Depth (m)	Salinity	Pot. temp. (θ) (°C)	Pot. dens. (σ_θ) (kg m^{-3})	Ce/Ce*	[Nd] $\pm 2\sigma$ (pmol kg^{-1})	$^{143}Nd/^{144}Nd \pm 2\sigma^1$	$\varepsilon_{Nd} \pm 2\sigma$	Water Mass
FLUSEC 43 (25 August 2007; 163°41′E, 17°32′S; depth, 3500 m)								
183	35.686	21.18	24.98	0.77	–	0.512570 ± 23	−1.8 ± 0.4	TW
241	35.591	18.94	25.50	0.55	–	0.512537 ± 20	−2.5 ± 0.4	
756	34.403	5.56	27.14	0.09	9.7 ± 0.2	0.512337 ± 44	−6.4 ± 0.9	AAIW
FLUSEC 22 (20 August 2007; 156°14′E, 10°58′S; depth, 3000 m)								
50	34.610	27.77	22.18	0.31	–	0.512711 ± 17	+0.9 ± 0.3	SW
171	35.744	21.06	25.06	0.27	–	0.512647 ± 16	−0.3 ± 0.3	TW
221	35.519	18.32	25.61	0.27	8.6 ± 0.2	0.512249 ± 25	−3.4 ± 0.5	
635	34.443	5.93	27.13	0.20	8.9 ± 0.1	0.512460 ± 24	−4.0 ± 0.5	AAIW
EUC-Fe 30 (30 September 2006; 147°42′E, 5°59′S; depth, 1040 m)								
25	34.575	27.30	22.30	0.37	–	0.512658 ± 14	−0.1 ± 0.3	SW
150	35.635	22.99	24.42	0.36	–	0.512624 ± 13	−0.8 ± 0.3	TW
200	35.570	19.25	25.39	0.58	–	0.512623 ± 30	−0.8 ± 0.6	TW
800	34.487	5.49	27.21	0.09	8.0 ± 0.1	0.512441 ± 20	−4.4 ± 0.4	AAIW
EUC-Fe 29 (28 September 2006; 145°28′E, 4°09′S; depth, 2089 m)								
40	34.724	27.32	22.41	0.36	–	0.512694 ± 20	+0.6 ± 0.4	SW
188	35.477	19.42	25.28	0.31	–	0.512609 ± 22	-1.1 ± 0.4	TW
320	35.059	13.31	26.37	0.17	–	0.512506 ± 05	-2.6 ± 0.1	CW
499	34.615	8.25	26.93	0.11	6.6 ± 0.1	–	–	SAMW
737	34.490	5.74	27.18	0.08	8.7 ± 0.1	0.512515 ± 12	-2.9 ± 0.2	AAIW
1300	34.574	3.42	27.51	0.08	12.4 ± 0.2	0.512601 ± 06	-0.7 ± 0.1	
2050	34.634	2.16	27.67	0.04	19.2 ± 0.2	–	–	UCDW
EUC-Fe 28 (27 September 2006; 143°52′E, 3°21′S; depth, 2252 m)								
40	34.706	27.63	22.29	0.48	8.4 ± 0.3	0.512754 ± 24	+2.3 ± 0.5	SW
100	34.853	26.49	22.77	0.32	8.6 ± 0.3	0.512723 ± 27	+1.7 ± 0.5	
191	35.461	19.27	25.30	0.26	2.6 ± 0.1	0.512598 ± 21	-0.8 ± 0.4	TW
320	35.099	13.79	26.31	0.17	5.6 ± 0.1	0.512579 ± 07	-1.2 ± 0.1	CW
500	34.613	8.21	26.94	0.17	8.4 ± 0.2	0.512510 ± 18	-2.5 ± 0.3	SAMW
800	34.496	5.53	27.21	0.12	9.3 ± 0.2	0.512531 ± 15	-2.1 ± 0.2	AAIW
1300	34.580	3.41	27.51	0.14	16.1 ± 0.3	0.512573 ± 17	-1.3 ± 0.3	
2000	34.626	2.35	27.64	0.08	19.2 ± 0.4	0.512602 ± 10	-0.7 ± 0.2	UCDW
EUC-Fe 26 (26 September 2006; 145°00′E, 2°00′N; depth, 4488 m)								
25	34.027	28.80	21.40	0.33	6.6 ± 0.4	–	–	SW
130	35.281	24.41	23.73	0.26	4.6 ± 0.8	0.512581 ± 05	−1.1 ± 0.1	
160	35.402	19.94	25.08	0.22	4.5 ± 0.4	0.512594 ± 05	−0.9 ± 0.1	TW
265	34.520	10.39	26.51	0.09	6.9 ± 0.2	0.512519 ± 05	−2.3 ± 0.1	CW
350	34.672	9.46	26.79	0.09	6.8 ± 0.6	–	–	
480	34.608	8.28	26.92	0.11	7.3 ± 1.1	0.512514 ± 05	−2.4 ± 0.1	SAMW
700	34.528	6.17	27.16	0.09	8.4 ± 0.7	–	–	EqIW
EUC-Fe 25 (25 September 2006; 149°30′E, 0°00′; depth, 3368 m)								
25	33.954	29.41	21.14	0.32	6.1 ± 0.6	0.512615 ± 07	−0.4 ± 0.1	SW
130	35.438	22.12	24.52	0.23	4.5 ± 0.3	0.512606 ± 07	−0.6 ± 0.1	TW
145	35.413	19.90	25.10	0.26	3.5 ± 0.4	0.512604 ± 06	−0.7 ± 0.1	TW
205	35.188	15.54	26.00	0.16	6.1 ± 0.4	0.512552 ± 08	−1.7 ± 0.2	
275	35.009	13.18	26.36	0.14	5.4 ± 0.4	0.512528 ± 04	−2.1 ± 0.1	CW
375	34.747	10.25	26.71	0.14	7.0 ± 0.6	0.512514 ± 07	−2.4 ± 0.1	SAMW
680	34.547	6.25	27.16	0.09	7.9 ± 0.4	0.512515 ± 05	−2.4 ± 0.1	
800	34.531	5.51	27.24	0.04	8.3 ± 0.9	0.512522 ± 05	−2.3 ± 0.1	EqIW
EUC-Fe 24 (23 September 2006; 152°29′E, 3°22′S; depth, 1673 m)								
40	34.567	28.76	21.82	0.31	5.8 ± 0.6	0.512721 ± 05	+1.6 ± 0.1	SW
150	35.588	22.56	24.51	0.25	4.4 ± 0.7	0.512631 ± 12	−0.1 ± 0.2	TW
200	35.451	17.60	25.72	0.26	5.3 ± 0.3	0.512552 ± 06	−1.7 ± 0.1	
285	35.033	13.03	26.41	0.24	5.6 ± 0.3	0.512521 ± 08	−2.3 ± 0.2	CW
370	34.725	9.91	26.75	0.09	6.8 ± 0.5	0.512512 ± 04	−2.5 ± 0.1	SAMW
700	34.535	6.32	27.14	0.08	7.7 ± 1.1	0.512498 ± 04	−2.7 ± 0.1	
800	34.520	5.31	27.26	0.06	8.6 ± 1.2	0.512498 ± 06	−2.7 ± 0.1	EqIW
1619	34.609	2.64	27.61	0.10	12.2 ± 0.6	0.512523 ± 04	−2.2 ± 0.1	
EUC-Fe 23 (22 September 2006; 156°00′E, 1°21′S; depth, 1997 m)								
50	34.639	29.29	21.70	0.28	4.2 ± 2.2	0.512613 ± 06	−0.5 ± 0.1	SW
140	35.688	23.34	24.36	0.31	3.5 ± 0.3	0.512581 ± 13	−1.1 ± 0.3	TW
185	35.548	20.16	25.14	0.25	3.7 ± 0.7	0.512584 ± 08	−1.0 ± 0.2	TW
220	35.238	15.23	26.10	0.16	3.9 ± 0.3	0.512506 ± 05	−2.6 ± 0.2	CW
220	35.238	15.23	26.10	0.18	4.3 ± 0.3	0.512499 ± 07	−2.7 ± 0.1	CW
220	35.238	15.23	26.10	0.17	4.4 ± 0.5	0.512501 ± 11	−2.7 ± 0.2	CW

-: not measured.

(*continues*)

Table 1. (continued)

Depth (m)	Salinity	Pot. temp. (θ) (°C)	Pot. dens. (σ_θ) (kg m^{-3})	Ce/Ce*	[Nd] $\pm 2\sigma$ (pmol kg^{-1})	^{143}Nd/^{144}Nd $\pm$ 2σ[1]	$\varepsilon_{Nd} \pm 2\sigma$	Water Mass
EUC-Fe 22 (21 September 2006; 156°00′E, 0°21′N; depth, 2048 m)								
20	33.930	29.70	21.03	0.30	6.7 ± 0.3	0.512626 ± 15	−0.2 ± 0.3	SW
140	35.202	20.03	24.91	0.21	5.1 ± 0.2	0.512570 ± 27	−1.3 ± 0.5	TW
190	35.305	17.25	25.69	0.20	5.0 ± 0.1	0.512582 ± 10	−1.1 ± 0.2	
260	34.825	12.23	26.41	0.14	7.2 ± 0.2	0.512538 ± 17	−2.0 ± 0.3	CW
385	34.744	10.08	26.74	0.14	7.3 ± 0.2	0.512467 ± 26	−3.3 ± 0.5	SAMW
500	34.605	8.09	26.95	0.28	9.3 ± 0.4	0.512413 ± 19	−4.4 ± 0.4	
640	34.554	6.49	27.14	0.08	8.6 ± 0.2	0.512526 ± 12	−2.2 ± 0.2	
800	34.532	5.32	27.27	0.08	8.6 ± 0.2	0.512490 ± 24	−2.9 ± 0.5	EqIW
EUC-Fe 21 (20 September 2006; 156°00′E, 2°00′N; depth, 2587 m)								
25	33.910	29.70	21.01	0.30	4.8 ± 0.3	–	–	SW
25	33.910	29.70	21.01	0.30	4.8 ± 0.4	–	–	SW
25	33.910	29.70	21.01	0.30	5.1 ± 0.4	–	–	SW
25	33.910	29.70	21.01	0.30	4.9 ± 0.4	–	–	SW
25	33.910	29.70	21.01	0.31	5.4 ± 0.4	0.512576 ± 06	−1.2 ± 0.1	SW
150	35.305	22.35	24.35	0.25	3.9 ± 0.4	0.512581 ± 05	−1.1 ± 0.1	TW
205	34.655	11.49	26.42	0.10	6.7 ± 0.5	0.512509 ± 08	−2.5 ± 0.1	CW
355	34.720	10.01	26.73	0.09	6.6 ± 0.6	0.512528 ± 04	−2.2 ± 0.1	SAMW
355	34.720	10.01	26.73	0.09	6.6 ± 0.7	0.512523 ± 04	−2.2 ± 0.1	SAMW
355	34.720	10.01	26.73	0.08	6.5 ± 2.7	0.512520 ± 04	−2.3 ± 0.1	SAMW
EUC-Fe 15 (11 September 2006; 180°00′E, 2°00′S; depth, 5389 m)								
15	34.484	30.24	21.26	0.25	4.0 ± 0.2	0.512593 ± 07	−0.9 ± 0.1	SW
75	35.486	29.20	22.36	0.33	3.5 ± 0.3	0.512571 ± 08	−1.3 ± 0.1	
145	35.981	24.42	24.26	0.19	3.3 ± 0.1	0.512540 ± 08	−1.9 ± 0.2	TW
185	35.346	16.33	25.94	0.16	4.0 ± 0.1	0.512536 ± 05	−2.0 ± 0.1	
400	34.742	10.20	26.72	0.08	4.9 ± 0.2	0.512525 ± 05	−2.2 ± 0.1	NPIW
850	34.537	5.52	27.25	0.09	7.0 ± 1.1	0.512512 ± 04	−2.5 ± 0.1	EqIW
EUC-Fe 14 (10 September 2006; 180°00′E, 0°00′; depth, 5222 m)								
15	34.660	30.35	21.35	0.23	4.0 ± 0.1	0.512573 ± 13	−1.3 ± 0.2	SW
97	35.320	29.84	22.02	0.19	4.5 ± 0.1	0.512558 ± 31	−1.6 ± 0.6	
140	35.612	23.15	24.35	0.21	5.2 ± 0.3	0.512557 ± 25	−1.6 ± 0.5	TW
160	35.071	19.50	24.95	0.21	5.2 ± 0.2	0.512543 ± 20	−1.9 ± 0.4	TW
172	35.455	19.05	25.36	0.19	5.8 ± 0.1	0.512549 ± 16	−1.7 ± 0.3	TW
204	34.840	14.60	25.94	0.16	7.0 ± 0.2	0.512558 ± 17	−1.6 ± 0.3	
400	34.692	9.38	26.81	0.07	7.3 ± 0.2	0.512563 ± 39	−1.5 ± 0.8	NPIW
850	34.545	5.34	27.27	0.07	8.7 ± 0.4	0.512499 ± 15	−2.7 ± 0.3	EqIW
2800	34.669	1.54	27.74	0.04	23.1 ± 0.6	0.512502 ± 11	−2.7 ± 0.2	UCDW
4000	34.693	1.12	27.79	0.03	28.1 ± 0.6	0.512363 ± 15	−5.4 ± 0.3	
5100	34.707	0.82	27.82	0.04	26.7 ± 1.0	0.512267 ± 13	−7.2 ± 0.3	LCDW
EUC-Fe 13 (9 September 9, 2006; 180°00′E, 2°00′N; depth, 5222 m)								
15	34.429	30.29	21.20	0.28	3.7 ± 0.2	0.512599 ± 07	−0.8 ± 0.1	SW
80	35.323	29.22	22.23	0.22	3.4 ± 0.2	0.512573 ± 06	−1.3 ± 0.1	
115	35.470	28.26	22.66	0.21	3.5 ± 0.2	0.512553 ± 06	−1.7 ± 0.1	
175	34.700	13.42	26.07	0.11	6.5 ± 0.4	0.512529 ± 05	−2.1 ± 0.1	
380	34.744	10.29	26.70	0.11	5.1 ± 0.5	0.512534 ± 06	−2.0 ± 0.1	NPIW
900	34.540	5.06	27.30	0.09	8.6 ± 0.3	0.512520 ± 04	−2.3 ± 0.1	EqIW
EUC-Fe 3 (27 August 2006; 140°00′W, 2°00′S; depth, 4260 m)								
15	35.566	26.86	23.19	0.20	3.5 ± 0.1	0.512568 ± 12	−1.4 ± 0.2	SW
60	35.504	26.86	23.14	0.21	3.6 ± 0.1	0.512577 ± 07	−1.2 ± 0.1	
110	35.938	22.31	24.84	0.20	3.5 ± 0.1	0.512492 ± 06	−2.8 ± 0.1	TW
200	34.925	12.83	26.37	0.11	5.7 ± 0.3	0.512545 ± 07	−1.8 ± 0.1	CW
480	34.671	8.94	26.87	0.10	6.9 ± 0.4	0.512535 ± 06	−1.4 ± 0.2	NPIW
928	34.546	4.99	27.32	0.07	7.9 ± 0.3	0.512531 ± 05	−2.1 ± 0.1	EqIW
EUC-Fe 2 (25 August 2006; 140°00′W, 0°00′; depth, 4330 m)								
15	35.334	26.48	23.13	0.22	3.7 ± 0.2	0.512580 ± 08	−1.1 ± 0.2	SW
50	35.362	26.24	23.23	0.21	3.7 ± 0.2	0.512552 ± 09	−1.7 ± 0.2	
90	35.451	25.89	23.41	0.21	3.9 ± 0.2	0.512555 ± 06	−1.6 ± 0.1	
110	35.559	24.88	23.80	0.20	4.9 ± 0.2	0.512546 ± 05	−1.8 ± 0.1	
130	35.014	21.03	24.50	0.19	4.6 ± 0.2	0.512537 ± 08	−2.0 ± 0.2	TW
250	34.924	12.93	26.35	0.11	5.8 ± 0.2	0.512539 ± 05	−1.9 ± 0.1	CW
400	34.721	9.79	26.77	0.10	6.6 ± 0.3	0.512543 ± 06	−1.9 ± 0.1	NPIW
850	34.548	5.40	27.27	0.08	8.0 ± 0.3	0.512529 ± 05	−2.1 ± 0.1	EqIW
EUC-Fe 1 (24 August 2006; 140°00′W, 2°00′N; depth, 4374 m)								
15	35.081	26.50	22.94	0.22	3.9 ± 0.9	0.512577 ± 07	−1.2 ± 0.1	SW
50	35.108	26.32	23.01	0.23	3.9 ± 1.1	0.512579 ± 10	−1.1 ± 0.2	
130	34.830	16.06	25.60	0.24	5.2 ± 0.2	0.512559 ± 10	−1.5 ± 0.2	
250	34.876	12.39	26.42	0.11	6.2 ± 0.5	0.512566 ± 08	−1.5 ± 0.2	CW
510	34.647	8.68	26.89	0.10	7.8 ± 0.7	0.512562 ± 05	−1.5 ± 0.1	NPIW
850	34.546	5.14	27.30	0.08	8.6 ± 0.3	0.512526 ± 05	−2.2 ± 0.1	EqIW

[1]Absolute errors of ^{143}Nd/^{144}Nd have to be multiplied by 10^{-6}.

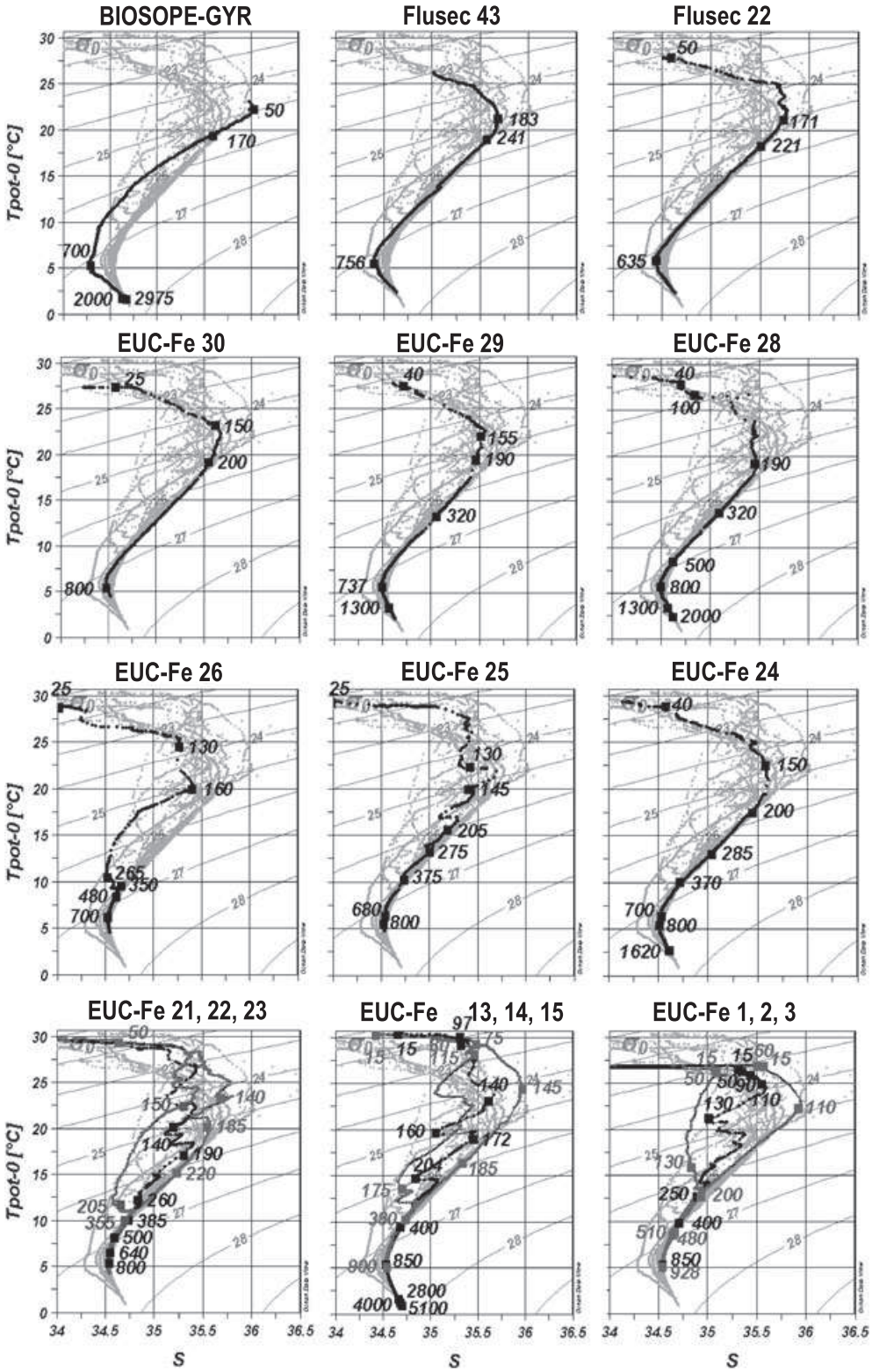

Figure 2. Potential temperature (θ)-salinity (S) plots for the stations indicated in Figure 1. The station associated with the bold black curve is indicated above each plot. In the background, grey curves represent the θ-S of all the stations studied here, illustrating the total θ-S range. Potential density contours are shown in solid grey. Each sample measured for Nd isotopes and REE concentrations is identified by its depth (m). For the stations along the equator (bottom row of panels), at 156°E, 180° and 140°W, the northern, equatorial, and southern stations are represented on the same plot. The northern and southern stations are easily distinguishable, being respectively poorly and highly salty within the thermocline (dark grey curves).

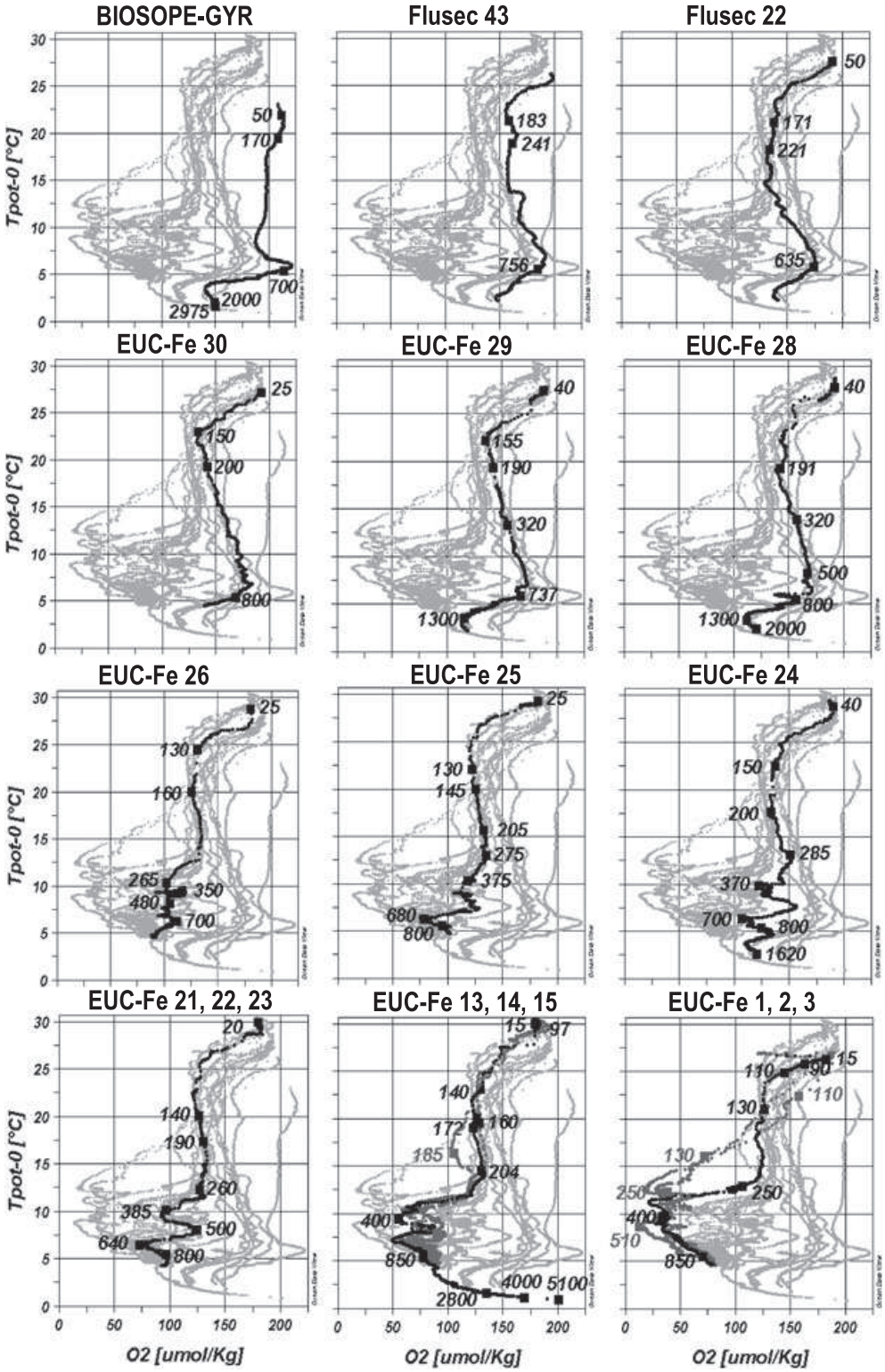

Figure 3. As Figure 2, but showing potential temperature (θ)-dissolved oxygen (O_2) plots. For the stations along the equator (bottom row of panels), at 180° and 140°W, the northern, equatorial, and southern stations are represented on the same plot. At 156°E-0°, northern, equatorial, and southern stations have a very similar θ-O_2 profile; we thus represented only the equatorial profile, for more clarity.

exhibit low salinity (~34.9) and high nutrient concentrations [*Tsuchiya et al.*, 1989]. Interleaving of northern- and southern-origin waters can be seen at equatorial stations on the three θ-S plots at the bottom of Figure 2.

[17] The Western South Pacific Central Water (WSPCW) [*Tomczak and Hao*, 1989] is centered on a potential density of 26.4 kg m^{-3}. This water mass is formed at the Subtropical Convergence, outcropping in winter in the Tasman Sea.

WSPCW exhibits high salinity (mean salinity, $\bar{S} = 35$), high oxygen (mean oxygen, $\bar{O}_2 = 160\ \mu mol\ kg^{-1}$), and low nutrient concentrations [*Tsuchiya et al*., 1989; *Sokolov and Rintoul*, 2000]. It is carried by the subtropical gyre and joins the Tropical Convergence zone, flowing underneath the Tropical Waters. It then reaches the Coral Sea via the northern branch of the subtropical gyre in the South Equatorial Current [*Qu and Lindstrom*, 2002]. WSPCW partly participates in the formation of Equatorial 13°C Water [*Tsuchiya*, 1981; *Qu et al.*, 2009].

[18] In the northern hemisphere, Western North Pacific Central Water (WNPCW) [*Tomczak and Godfrey*, 2003] is a low-salinity, low-oxygen, high-nutrient water. Formed and subducted in the northern Subtropical Convergence, it is carried in our region by the eastward North Equatorial Countercurrent (NECC) and EUC.

3.2. Subantarctic Mode Water and Intermediate Waters

[19] Subantarctic Mode Water (SAMW) [*McCartney*, 1977; *Sokolov and Rintoul*, 2000] overlies Antarctic Intermediate Water (AAIW), just below the lower part of the thermocline. SAMW originates from the southeastern Pacific, being formed by deep winter convection. This water mass is centered on $\sigma_\theta = 27.07\ kg\ m^{-3}$ at its source and is characterized by a low salinity (~34.5) and a high oxygen pycnostad. During its equatorward transit, and mainly along the LLWBCs, SAMW undergoes diapycnal mixing with underlying waters and participates in the formation of Equatorial 13°C Water [*Qu et al.*, 2009].

[20] North Pacific Intermediate Water (NPIW; $\sigma_\theta = 26.5$–$27.2\ kg\ m^{-3}$) originates in the western North Pacific [*Talley*, 1993; *You*, 2003]. This water mass is poorly oxygenated (0–$150\ \mu mol\ kg^{-1}$) and is characterized by a salinity minimum (~33.8). It follows an anticyclonic circulation in the North Pacific, flowing between 300 m and 800 m depth, and mainly exits into the Celebes Sea through the Mindanao Current [*Bingham and Lukas*, 1994; *Fine et al*., 1994; *You et al*., 2003]. The hypothetical occurrence of a modified NPIW in the equatorial Pacific is discussed in section 4.

[21] The AAIW ($\sigma_\theta = 27.1\ kg\ m^{-3}$) is formed in the southeast Pacific Ocean and is linked to the formation of the densest SAMW [*Tsuchiya and Talley*, 1998; *Bostock et al*., 2010]. Highly oxygenated ($O_2 = 200$–$300\ \mu mol\ kg^{-1}$) and relatively fresh (S = 34.3–34.5) [*Tsuchiya and Talley*, 1996], AAIW flows between 600 m and 1400 m depth and is conveyed within the subtropical gyre and then toward the Coral Sea [*Gasparin et al*., 2011]. The water mass is then conveyed by the intermediate New Guinea Coastal Undercurrent [*Reid*, 1997; *Sokolov and Rintoul*, 2000; *Qu and Lindstrom*, 2004; *Bostock et al*., 2010]. Finally, AAIW reaches the equator north of New Guinea [*Tsuchiya*, 1991; *Fine et al*., 1994; *Qu and Lindstrom*, 2004; *Zenk et al*., 2005]. From the Coral Sea to the equator, AAIW is slightly denser than at its source ($\sigma_\theta = 27.26\ kg\ m^{-3}$) and exhibits lower oxygen concentrations (160–$190\ \mu mol\ kg^{-1}$) [*Tsuchiya*, 1991]. AAIW is identified at five stations of our study: the two FLUSEC stations and the three stations along the PNG coast, from the EUC-Fe cruise (Table 1 and Figures 2 and 8).

[22] Equatorial Pacific Intermediate Water (EqPIW; $\sigma_\theta = 27.3\ kg\ m^{-3}$) is primarily a combination of AAIW and upwelling Pacific Deep Water [*Bostock et al*., 2010]. It displays the highest salinities (34.5–34.6) among the three intermediate waters. EqPIW is subdivided into north and south components that exhibit very low oxygen concentrations, respectively, in the ranges 0–$75\ \mu mol\ kg^{-1}$ and 75–$125\ \mu mol\ kg^{-1}$. These waters flow within a complex intermediate current system. Between 1°S and 1°N, they are conveyed by the Lower Equatorial Intermediate Current (L-EIC; 600–1200 m depth), a non-permanent westward current that reverses into an eastward current in boreal spring [*Marin et al*., 2010]. Between 1° and 4° latitude north and south of the equator, the EqPIW flows within a series of extraequatorial eastward and westward jets [*Firing et al*., 1998; *Cravatte et al*., 2012]. Nine EqPIW samples were collected during the EUC-Fe cruise, within the area (149°E-140°W) and (4°S-2°N) (Figure 2). In the following, AAIW and the EqIW will be grouped under a single overall denomination "Intermediate Waters" (IW).

3.3. Deep Waters

[23] Upper Circumpolar Deep Water (UCDW) flows between 1000 and 2000 m depth within the Antarctic Circumpolar Current (ACC) above Lower CDW (LCDW), centered on $\sigma_\theta = 27.65\ kg\ m^{-3}$ [*Orsi et al*., 1995]. This water mass is characterized by relatively low oxygen (from $170\ \mu mol\ kg^{-1}$ in the Southern Ocean to $120\ \mu mol\ kg^{-1}$ in our region) and high nutrient concentrations [*Callahan*, 1972]. UCDW pathways are still only approximately understood. From Reid's observations [*Reid*, 1997], from Figure 2c of *Tsimplis et al*. [1998], and from Figure 2b of *Kawabe and Fujio* [2010], UCDW detaches from the ACC southeast of New Zealand and is conveyed by the anticyclonic flow in the South Pacific, detouring around the subtropical gyre and reaching the equatorial western Pacific. Its occurrence and fate within the Coral and Solomon Seas are poorly documented. It mainly upwells in the Philippine Sea and mixes with the North Pacific Deep Water (NPDW) and LCDW to form a modified NPDW. UCDW was collected at four stations (see Table 1).

[24] The dominant deep and bottom water of the South Pacific is LCDW ($\sigma > 45.86\sigma_4$). LCDW is a remnant of North Atlantic Deep Water (NADW) and thus is characterized by a salinity maximum (S = 34.72–34.73) and a silicate minimum [*Orsi et al*., 1999]. This deep water flows from the ACC toward the North Pacific via complex pathways [see *Sokolov and Rintoul*, 2000 and Figure 2c of *Kawabe and Fujio*, 2010]. In the mid and high-latitude North Pacific, LCDW upwells in the upper deep layers and is transformed into NPDW [*Reid*, 1997; *Kawabe and Fujio*, 2010]. In our study, this water mass is characterized at one point only, thanks to a 5100 m depth sample collected at station 14.

4. Results

4.1. Nd Concentration and Isotopic Composition Results

[25] The ε_{Nd}, Nd concentrations [Nd], θ and S data as well as σ_θ are compiled in Table 1; O_2 data can be found in Table 2 together with S and σ_θ, reproduced in this table

Table 2. Dissolved REE Concentrations Measured in Our Samples (in pmol kg^{-1})

Depth(m)	Salinity	O_2 (μmol kg^{-1})	σ_θ (kg m^{-3})	La	Ce	Pr	Nd	Sm	Eu	Gd	Tb	Dy	Ho	Er	Tm	Yb	Lu
FLUSEC 43 (25 August 2007; 163°41′E, 17°32′S; depth, 3500 m)																	
183	35.686	159	24.98	–	–	–	–	–	–	–	–	–	–	–	–	–	–
241	35.591	162	25.50	–	–	–	–	–	–	–	–	–	–	–	–	–	–
756	34.403	185	27.14	15.68	7.10	2.29	9.72	1.70	0.47	2.53	0.39	3.33	1.01	3.78	0.57	3.71	0.67
FLUSEC 22 (20 August 2007; 156°14E, 10°58′S; depth, 3000 m)																	
50	34.610	192	22.18	–	–	–	–	–	–	–	–	–	–	–	–	–	–
171	35.744	138	25.06	–	–	–	–	–	–	–	–	–	–	–	–	–	–
221	35.519	135	25.61	10.39	4.99	1.86	8.55	1.79	0.50	2.72	0.42	3.34	0.90	3.08	0.41	2.51	0.42
635	34.443	174	27.13	15.40	5.67	2.04	8.94	1.46	0.49	2.59	0.40	3.51	1.07	4.01	0.61	3.96	0.73
EUC-Fe 30 (30 September 2006; 147°42′E, 5°59′S; depth, 1040 m)																	
25	34.575	194	22.30	–	–	–	–	–	–	–	–	–	–	–	–	–	–
150	35.635	133	24.42	–	–	–	–	–	–	–	–	–	–	–	–	–	–
200	35.570	142	25.39	–	–	–	–	–	–	–	–	–	–	–	–	–	–
800	34.487	169	27.21	13.69	1.58	1.69	8.01	1.47	0.49	2.62	0.43	3.61	1.09	4.16	0.62	4.15	0.76
EUC-Fe 29 (28 September 2006; 145°28′E, 4°09′S; depth, 2089 m)																	
40	34.724	187	22.41	–	–	–	–	–	–	–	–	–	–	–	–	–	–
188	35.477	142	25.28	–	–	–	–	–	–	–	–	–	–	–	–	–	–
320	35.059	156	26.37	–	–	–	–	–	–	–	–	–	–	–	–	–	–
499	34.615	171	26.93	10.35	1.48	1.38	6.56	1.26	0.38	2.23	0.35	3.11	0.93	3.51	0.52	3.37	0.61
737	34.490	167	27.18	14.10	2.79	1.86	8.74	1.61	0.51	2.81	0.42	3.80	1.15	4.30	0.65	4.34	0.80
1300	34.574	116	27.51	19.63	2.07	2.54	12.39	2.40	0.75	4.16	0.61	5.38	1.57	5.87	0.87	6.09	1.15
2050	34.634	119	27.67	30.78	1.48	3.94	19.16	3.76	1.17	6.22	0.91	7.56	2.16	7.79	1.16	8.10	1.52
EUC-Fe 28 (27 September 2006; 143°52′E, 3°21′S; depth, 2252 m)																	
40	34.706	192	22.29	7.69	7.64	1.78	8.35	1.92	0.53	2.82	0.42	3.24	0.78	2.47	0.31	1.87	0.29
100	34.853	180	22.77	11.21	6.37	1.79	8.58	1.81	0.50	2.87	0.43	3.46	0.91	2.99	0.39	2.22	0.35
191	35.461	143	25.30	3.14	1.47	0.54	2.56	0.51	0.12	0.84	0.12	1.10	0.32	1.06	0.13	0.83	0.15
320	35.099	157	26.31	8.28	2.43	1.21	5.62	1.04	0.26	1.81	0.28	2.57	0.72	2.59	0.35	2.24	0.39
500	34.613	169	26.94	12.84	3.74	1.85	8.37	1.58	0.39	2.62	0.40	3.47	1.02	3.57	0.53	3.47	0.62
800	34.496	156	27.21	15.44	2.88	1.98	9.25	1.68	0.44	2.97	0.45	4.17	1.20	4.57	0.71	4.67	0.85
1300	34.580	113	27.51	25.38	6.00	3.45	16.11	3.27	0.86	5.16	0.76	6.36	1.79	6.44	0.97	6.72	1.24
2000	34.626	120	27.64	30.94	3.80	4.06	19.18	3.59	0.93	5.94	0.89	7.42	2.10	7.66	1.14	8.11	1.51
EUC-Fe 26 (26 September 2006; 145°00′E, 2°00′N; depth, 4488 m)																	
25	34.027	181	21.40	5.88	4.08	1.39	6.61	1.60	0.58	2.33	0.36	2.71	0.68	2.20	0.29	1.72	0.26
130	35.281	132	23.73	5.78	2.75	1.01	4.56	1.05	0.38	1.57	0.25	1.98	0.54	1.84	0.25	1.48	0.23
160	35.402	126	25.08	5.56	2.19	0.96	4.53	1.00	0.34	1.57	0.25	1.98	0.55	1.90	0.26	1.58	0.26
265	34.520	102	26.51	10.67	1.57	1.51	6.86	1.40	0.46	2.31	0.36	3.00	0.84	2.97	0.42	2.78	0.46
350	34.672	117	26.79	10.79	1.58	1.54	6.83	1.47	0.48	2.40	0.37	3.16	0.91	3.31	0.49	3.35	0.59
480	34.608	106	26.92	10.94	1.97	1.60	7.29	1.49	0.51	2.40	0.38	3.20	0.95	3.50	0.53	3.65	0.64
700	34.528	112	27.16	13.55	2.13	1.89	8.39	1.74	0.64	2.69	0.44	3.62	1.08	4.05	0.62	4.39	0.79
EUC-Fe 25 (25 September 2006; 149°30′E, 0°00′; depth, 3368 m)																	
25	33.954	182	21.14	6.00	3.73	1.23	6.12	1.45	0.48	2.25	0.36	2.69	0.68	2.21	0.29	1.70	0.26
130	35.438	123	24.52	5.30	2.26	0.93	4.47	0.98	0.34	1.58	0.25	2.01	0.55	1.88	0.25	1.51	0.24
145	35.413	126	25.10	4.31	2.09	0.76	3.52	0.78	0.25	1.37	0.21	1.83	0.52	1.79	0.24	1.40	0.23
205	35.188	133	26.00	8.49	2.40	1.34	6.09	1.32	0.46	2.08	0.33	2.64	0.73	2.52	0.35	2.21	0.37
275	35.009	135	26.36	7.94	1.94	1.25	5.45	1.22	0.42	1.90	0.30	2.52	0.71	2.55	0.36	2.38	0.40
375	34.747	118	26.71	12.20	2.73	1.53	7.00	1.36	0.41	2.29	0.36	2.98	0.87	3.14	0.46	3.03	0.54
680	34.547	79	27.16	13.37	1.95	1.81	7.90	1.60	0.60	2.48	0.41	3.47	1.03	3.98	0.60	4.27	0.78
800	34.531	95	27.24	37.72	1.84	1.87	8.33	1.70	0.64	2.72	0.44	3.74	1.13	4.31	0.66	4.70	0.86
EUC-Fe 24 (23 September 2006; 152°29′E, 3°22′S; depth, 1673 m)																	
40	34.567	190	21.82	5.19	3.22	1.15	5.78	1.40	0.51	2.23	0.35	2.59	0.68	2.19	0.29	1.61	0.27
150	35.588	137	24.51	5.28	2.44	0.92	4.44	1.01	0.38	1.64	0.27	2.04	0.57	1.94	0.28	1.58	0.27
200	35.451	133	25.72	7.64	3.47	1.19	5.29	1.06	0.34	1.61	0.25	2.10	0.61	2.22	0.32	2.10	0.37
285	35.033	153	26.41	7.28	3.10	1.24	5.64	1.19	0.43	1.84	0.29	2.40	0.69	2.45	0.34	2.13	0.36
370	34.725	125	26.75	10.15	1.62	1.48	6.78	1.39	0.50	2.14	0.34	2.92	0.85	3.14	0.47	3.18	0.56
700	34.535	109	27.14	12.07	1.61	1.69	7.72	1.57	0.57	2.51	0.40	3.50	1.05	4.02	0.61	4.33	0.77
800	34.520	125	27.26	19.11	1.72	1.91	8.64	1.74	0.63	2.81	0.44	3.91	1.17	4.49	0.69	4.91	0.89
1619	34.609	120	27.61	20.89	3.42	2.79	12.16	2.37	0.88	3.77	0.62	5.14	1.53	5.76	0.89	6.44	1.19
EUC-Fe 23 (22 September 2006; 156°00′E, 1°21′S; depth, 1997 m)																	
50	34.639	183	21.70	4.30	2.36	0.86	4.24	0.96	0.31	1.61	0.25	1.97	0.52	1.71	0.22	1.19	0.18
140	35.688	122	24.36	4.53	2.48	0.76	3.52	0.75	0.24	1.26	0.20	1.65	0.47	1.63	0.22	1.25	0.20
185	35.548	124	25.14	4.59	2.12	0.81	3.70	0.86	0.31	1.35	0.21	1.78	0.50	1.77	0.24	1.44	0.23
220	35.238	121	26.10	6.14	1.68	0.90	3.93	0.81	0.30	1.28	0.22	1.93	0.58	2.12	0.30	1.91	0.32
220	35.238	121	26.10	6.71	2.00	0.98	4.32	0.89	0.33	1.39	0.23	1.95	0.58	2.15	0.30	1.95	0.33
220	35.238	121	26.10	6.77	1.99	1.01	4.43	0.90	0.32	1.41	0.23	1.98	0.58	2.14	0.30	1.96	0.33
EUC-Fe 22 (21 September 2006; 156°00′E, 0°21′N; depth, 2048 m)																	
20	33.930	179	21.03	6.59	3.95	1.39	6.73	1.50	0.40	2.39	0.37	2.75	0.71	2.23	0.28	1.70	0.27
140	35.202	126	24.91	7.19	2.59	1.05	5.09	1.06	0.27	1.74	0.25	2.15	0.59	2.02	0.25	1.51	0.26
190	35.305	131	25.69	6.68	2.36	1.03	5.03	1.01	0.24	1.66	0.24	2.18	0.61	2.04	0.29	1.64	0.29
260	34.825	127	26.41	10.76	2.54	1.57	7.16	1.42	0.36	2.34	0.37	3.06	0.86	3.09	0.44	2.77	0.48

(*continues*)

Table 2. (continued)

Depth(m)	Salinity	O_2 (μmol kg^{-1})	σ_θ (kg m^{-3})	La	Ce	Pr	Nd	Sm	Eu	Gd	Tb	Dy	Ho	Er	Tm	Yb	Lu
385	34.744	98	26.74	13.00	2.93	1.70	7.26	1.31	0.34	2.48	0.38	3.38	0.97	3.57	0.53	3.39	0.61
500	34.605	125	26.95	6.45	4.22	1.89	9.26	2.18	0.49	2.43	0.38	3.46	0.95	3.41	0.62	4.46	0.81
640	34.554	73	27.14	15.12	1.86	1.83	8.62	1.54	0.37	2.71	0.43	3.68	1.12	4.13	0.60	4.10	0.76
800	34.532	96	27.27	16.37	2.05	1.95	8.59	1.75	0.43	3.02	0.48	4.14	1.22	4.63	0.69	4.77	0.90
EUC-Fe 21 (20 September 2006; 156°00′E, 2°00′N; depth, 2587 m)																	
25	33.910	182	21.01	4.73	2.85	1.01	4.85	1.14	0.38	1.92	0.30	2.34	0.61	2.00	0.27	1.55	0.24
25	33.910	182	21.01	4.73	2.81	1.00	4.77	1.16	0.37	1.91	0.30	2.32	0.61	2.00	0.26	1.55	0.24
25	33.910	182	21.01	4.90	2.95	1.06	5.09	1.24	0.41	1.99	0.31	2.41	0.63	2.05	0.27	1.59	0.24
25	33.910	182	21.01	4.73	2.84	1.02	4.91	1.20	0.39	1.92	0.30	2.33	0.61	1.98	0.26	1.53	0.23
25	33.910	182	21.01	5.17	3.22	1.11	5.37	1.31	0.45	2.00	0.31	2.43	0.62	2.03	0.27	1.57	0.24
150	35.305	122	24.35	4.60	2.08	0.79	3.86	0.92	0.33	1.60	0.23	1.97	0.54	1.89	0.25	1.51	0.24
205	34.655	116	26.42	10.68	1.77	1.46	6.74	1.36	0.43	2.40	0.38	3.08	0.86	3.04	0.43	2.79	0.47
355	34.720	94	26.73	9.44	1.47	1.43	6.55	1.34	0.46	2.13	0.34	2.86	0.84	3.11	0.46	3.12	0.55
355	34.720	94	26.73	10.41	1.58	1.46	6.61	1.35	0.47	2.14	0.33	2.88	0.85	3.15	0.46	3.14	0.56
355	34.720	94	26.73	10.33	1.32	1.39	6.53	1.32	0.42	2.17	0.34	2.90	0.85	3.14	0.47	3.13	0.55
EUC-Fe 15 (11 September 2006; 180°00′E, 2°00′S; depth, 5389 m)																	
15	34.484	181	21.26	4.09	1.99	0.80	3.98	0.91	0.30	1.52	0.23	1.84	0.49	1.59	0.20	1.05	0.16
75	35.486	190	22.36	4.56	2.74	0.77	3.51	0.76	0.27	1.26	0.19	1.62	0.44	1.48	0.17	0.94	0.14
145	35.981	137	24.26	4.81	1.51	0.70	3.33	0.69	0.26	1.14	0.18	1.56	0.45	1.61	0.21	1.22	0.20
185	35.346	105	25.94	5.42	1.55	0.87	3.97	0.84	0.32	1.42	0.23	1.95	0.58	2.12	0.30	1.91	0.33
400	34.742	77	26.72	9.32	1.20	1.06	4.91	0.94	0.37	1.98	0.33	2.82	0.83	3.11	0.46	3.10	0.54
850	34.537	83	27.25	11.13	1.69	1.55	7.02	1.56	0.60	2.56	0.42	3.61	1.09	4.24	0.65	4.66	0.85
EUC-Fe 14 (10 September 2006; 180°00′E, 0°00′; depth, 5222 m)																	
15	34.660	178	21.35	4.43	1.92	0.85	4.00	0.87	0.26	1.44	0.22	1.76	0.49	1.59	0.19	0.96	0.15
97	35.320	181	22.02	4.97	1.77	0.92	4.46	0.85	0.24	1.51	0.24	1.99	0.55	1.76	0.21	1.25	0.19
140	35.612	130	24.35	6.84	2.55	1.12	5.20	1.06	0.27	1.79	0.28	2.24	0.61	2.11	0.27	1.61	0.29
160	35.071	129	24.95	7.19	2.58	1.13	5.20	0.95	0.27	1.80	0.28	2.29	0.67	2.09	0.30	1.74	0.30
172	35.455	123	25.36	6.10	2.22	1.21	5.81	1.23	0.34	1.90	0.29	2.41	0.66	2.33	0.31	2.02	0.35
204	34.840	130	25.94	10.14	2.70	1.48	6.95	1.34	0.33	2.25	0.34	2.83	0.81	2.76	0.39	2.32	0.40
400	34.692	55	26.81	12.88	1.49	1.57	7.28	1.43	0.35	2.38	0.38	3.38	0.96	3.59	0.52	3.36	0.62
850	34.545	78	27.27	16.03	1.78	1.87	8.71	1.44	0.37	2.90	0.45	3.91	1.19	4.38	0.69	4.55	0.85
2800	34.669	135	27.74	41.07	2.54	5.09	23.11	4.32	0.97	6.74	1.02	8.61	2.43	8.82	1.35	9.43	1.71
4000	34.693	169	27.79	46.38	2.47	6.27	28.08	4.90	1.26	7.59	1.13	9.45	2.61	9.08	1.38	9.50	1.75
5100	34.707	201	27.82	42.83	2.94	6.00	26.68	4.86	1.15	7.18	1.09	8.56	2.33	8.10	1.23	8.51	1.56
EUC-Fe 13 (9 September 2006; 180°00′E, 2°00′N; depth, 5222 m)																	
15	34.429	182	21.20	4.16	2.18	0.76	3.73	0.86	0.33	1.43	0.22	1.74	0.47	1.52	0.19	0.98	0.15
80	35.323	180	22.23	3.92	1.55	0.69	3.43	0.74	0.25	1.30	0.20	1.68	0.47	1.59	0.20	1.13	0.17
115	35.470	156	22.66	4.25	1.60	0.73	3.53	0.80	0.30	1.30	0.21	1.71	0.48	1.66	0.22	1.23	0.19
175	34.700	129	26.07	9.49	1.78	1.43	6.48	1.37	0.47	2.16	0.34	2.79	0.78	2.77	0.39	2.55	0.43
380	34.744	59	26.70	7.36	1.39	1.13	5.10	1.17	0.47	2.05	0.34	2.83	0.84	3.13	0.47	3.17	0.56
900	34.540	88	27.30	15.15	2.09	1.94	8.56	1.77	0.68	2.78	0.47	3.86	1.16	4.47	0.69	4.92	0.89
EUC-Fe 3 (27 August 2006; 140°00′W, 2°00′S; depth, 4260 m)																	
15	35.566	173	23.19	4.39	1.58	0.72	3.53	0.74	0.25	1.29	0.21	1.69	0.48	1.63	0.21	1.19	0.19
60	35.504	190	23.14	4.28	1.65	0.76	3.62	0.80	0.30	1.31	0.21	1.70	0.48	1.65	0.22	1.22	0.19
110	35.938	158	24.84	4.52	1.63	0.74	3.46	0.70	0.26	1.14	0.18	1.48	0.44	1.51	0.19	1.09	0.18
200	34.925	21	26.37	9.40	1.72	1.29	5.70	1.16	0.43	1.83	0.30	2.47	0.73	2.68	0.40	2.66	0.46
480	34.671	30	26.87	12.08	1.97	1.59	6.92	1.39	0.51	2.19	0.35	2.99	0.89	3.33	0.50	3.47	0.62
928	34.546	80	27.32	14.30	1.57	1.77	7.90	1.58	0.58	2.63	0.42	3.72	1.15	4.44	0.69	4.94	0.90
EUC-Fe 2 (25 August 2006; 140°00′W, 0°00′; depth, 4330 m)																	
15	35.334	183	23.13	4.53	1.77	0.77	3.69	0.78	0.27	1.34	0.21	1.75	0.49	1.66	0.22	1.25	0.20
50	35.362	180	23.23	4.61	1.71	0.77	3.74	0.80	0.27	1.38	0.22	1.79	0.50	1.72	0.22	1.28	0.21
90	35.451	164	23.41	4.77	1.78	0.78	3.91	0.78	0.25	1.40	0.22	1.83	0.52	1.78	0.24	1.36	0.22
110	35.559	145	23.80	5.83	2.16	1.00	4.90	1.04	0.32	1.76	0.28	2.25	0.61	2.11	0.29	1.75	0.29
130	35.014	127	24.50	6.28	2.12	0.97	4.65	0.97	0.31	1.63	0.26	2.12	0.60	2.09	0.29	1.79	0.30
250	34.924	107	26.35	8.93	1.73	1.29	5.80	1.23	0.43	1.94	0.31	2.60	0.75	2.72	0.40	2.61	0.45
400	34.721	34	26.77	10.52	1.77	1.49	6.63	1.31	0.45	2.15	0.34	2.91	0.85	3.19	0.48	3.23	0.57
850	34.548	71	27.27	14.60	1.97	1.83	8.05	1.66	0.65	2.59	0.43	3.65	1.12	4.26	0.66	4.71	0.86
EUC-Fe 1 (24 August 2006; 140°00′W, 2°00′N; depth, 4374 m)																	
15	35.081	186	22.94	4.64	1.85	0.81	3.94	0.81	0.26	1.42	0.22	1.79	0.50	1.68	0.22	1.20	0.19
50	35.108	186	23.01	4.50	1.92	0.81	3.87	0.80	0.26	1.37	0.21	1.76	0.49	1.67	0.22	1.21	0.19
130	34.830	72	25.60	8.32	3.29	1.16	5.23	1.02	0.34	1.68	0.26	2.21	0.63	2.24	0.32	1.99	0.33
250	34.876	38	26.42	10.12	1.85	1.38	6.15	1.20	0.41	1.97	0.31	2.64	0.77	2.84	0.42	2.81	0.49
510	34.647	14	26.89	13.55	2.08	1.71	7.85	1.50	0.46	2.49	0.39	3.27	0.96	3.57	0.54	3.64	0.64
850	34.546	78	27.30	15.45	1.89	1.99	8.61	1.67	0.61	2.75	0.47	3.84	1.17	4.48	0.69	4.90	0.90

for easier reading. Figures 4 to 9 present the ε_{Nd} values, Nd concentrations and hydrographic properties (salinity and oxygen contents) for each water mass discussed here. The mean and maximum analytical precisions (2σ) of the reported data are 0.2 and 0.9 for ε_{Nd} and 0.4 and 2.7 pmol kg^{-1} for Nd concentrations, respectively (Table 1). In order not to overload the figures and the text, the analytical precisions are not given for each measurement. In the following,

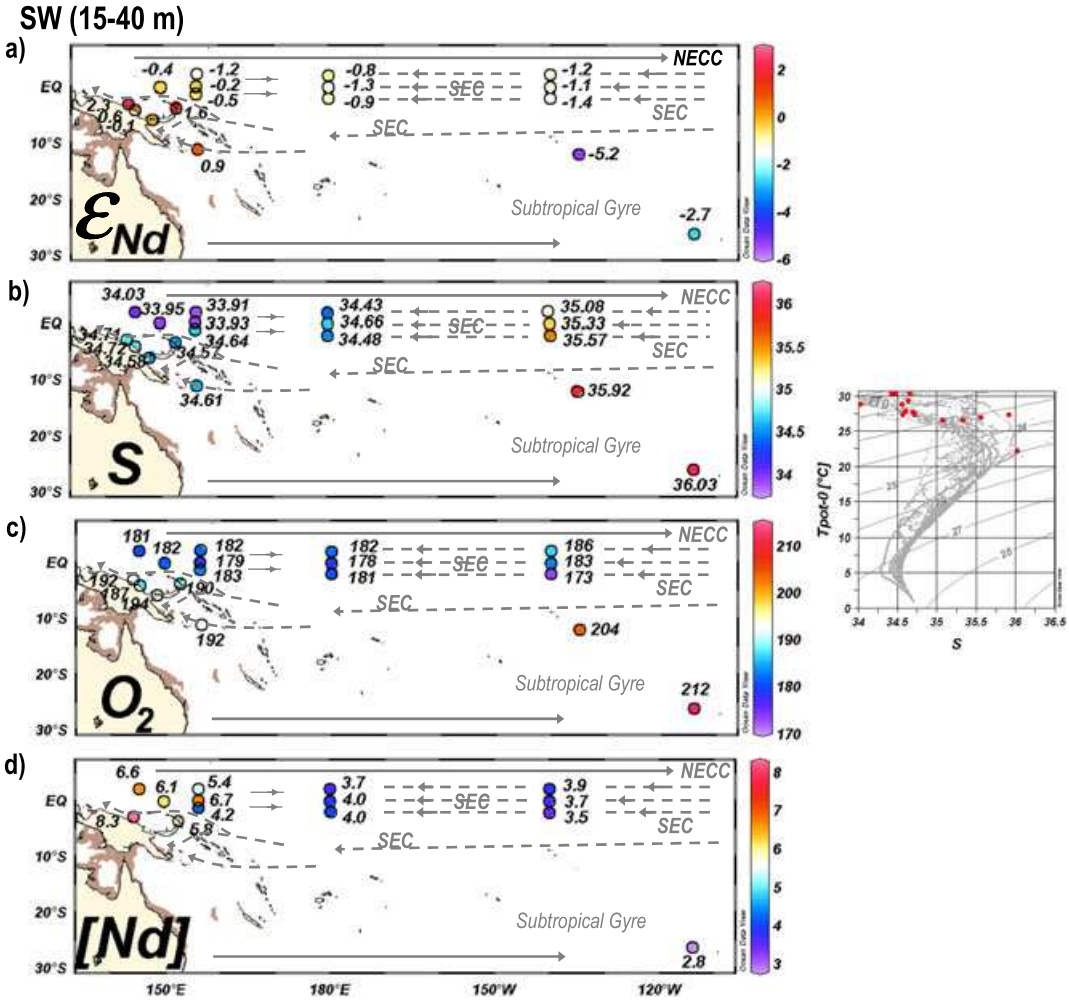

Figure 4. Neodymium data and hydrographic properties for surface waters (depth = 15–40 m), identified by red dots on the adjacent θ-S plot. (a) ε_{Nd}, (b) salinity, (c) dissolved oxygen (μmol kg^{-1}) and (d) Nd concentration (pmol kg^{-1}) are plotted at each station where surface waters were sampled. Currents are determined from ORCA025 climatology of September, corresponding to EUC-Fe cruise period, from *Reverdin et al*. [1994] and from *Hristrova and Kessler* [2012]. They are represented by grey arrows (dashed arrows = westward equatorial currents). The bathymetry shallower than 50 m appears in brown.

only the significant variations, that is, those beyond analytical precision, will be discussed. Note also that EUC-Fe 3, 15 and 23 will be discussed as the "2°S stations." Similarly, the "2°N stations" will refer to EUC-Fe 1, 13 and 21 and the "0° stations" will refer to EUC-Fe 2, 14 and 22.

4.1.1. Surface Waters

[26] Surface waters (SW) undergo continual hydrological modification due to interactions with the atmosphere. Therefore, only the main surface currents described in previous work are represented in Figure 4 [*Reverdin et al*., 1994; *Lagerloef et al*., 1999; *Johnson*, 2001; OSCAR, http://www.oscar.noaa.gov/].

[27] The ε_{Nd} distribution in surface waters allows two areas to be distinguished (Figure 4a):

1. Less radiogenic SW is found within the subtropical gyre, particularly at station EqPac in the HSEA (Figure 1) [*Lacan and Jeandel*, 2001]. The ε_{Nd} of SW at the 2°N, 2°S and 0° stations are all slightly negative, ranging from −1.4 to −0.2. The salinity data illustrate the contrast between the fresh warm pool in the westernmost equatorial region extending to 180° and the saltier cold tongue east of the dateline (Figure 4b). The cold tongue is associated with lower and more constant ε_{Nd} (Figure 4a) and Nd concentrations (Figure 4d) than the warm pool.
2. The more radiogenic SW is found along the coasts of PNG and New Ireland and within the Solomon Sea. Notably, ε_{Nd} of SW sampled at station EUC-Fe 28 (+2.3, downstream of the Sepik River) and at station EUC-Fe 24 (+1.6) are the highest values published so far for this region [*Lacan et al*., 2012]. The SW samples collected along the coasts of PNG and New Ireland also exhibit high Nd concentrations (5.8–8.3 pmol kg^{-1}; Figure 4d).

4.1.2. Thermocline Waters

4.1.2.1. Tropical Waters

[28] The distribution of ε_{Nd} values in Tropical Waters (TW) defines three distinct regions (Figure 5a).

1. From the subtropical gyre to the Coral and Solomon Seas, ε_{Nd} of TW increases from −4.3 to −0.3. Salinity and

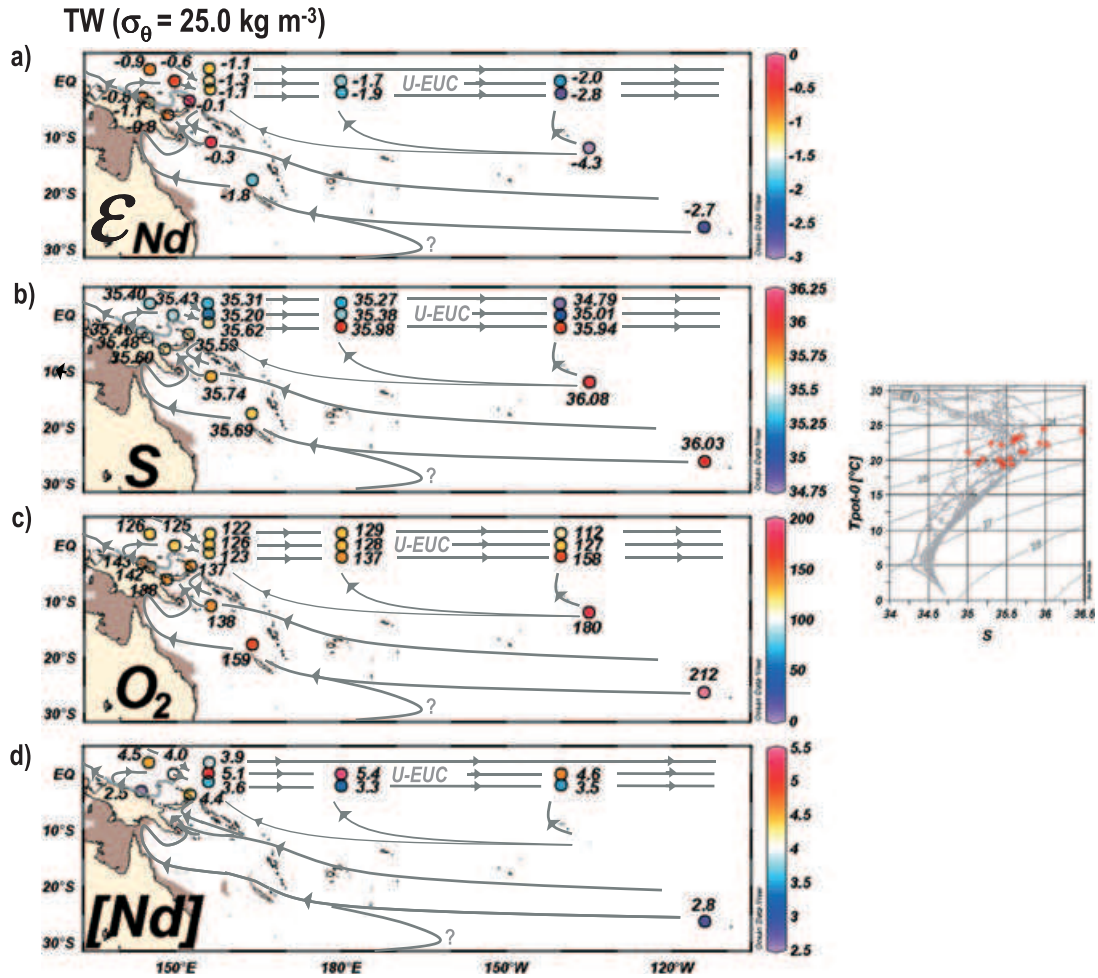

Figure 5. As Figure 4, for Tropical Waters ($\bar{\sigma}_\theta = 25.0\,\mathrm{kg\,m^{-3}}$), except that current pathways are built on both literature and hydrological and geochemical data measured at our stations. The bathymetry shallower than 100 m is colored in dark brown, in light brown if shallower than 250 m.

oxygen concentrations are relatively high and heterogeneous ($S > 35.6$, $O_2 > 135\ \mu\mathrm{mol\,kg^{-1}}$; Figures 5b and 5c).

2. From the Solomon Sea to the equator, ε_{Nd} values are rather homogeneous, on average equal to -0.7 ± 0.3 ($n = 7$). This area presents the most radiogenic TW among the three regions, particularly within the Solomon Sea (station FLUSEC 22), along the coasts of New Ireland (station EUC-Fe 24) and at the equator (station EUC-Fe 25). Oxygen concentrations and salinity are also relatively homogeneous, decreasing slightly northward, and illustrating weak intrusions of TW of northern hemisphere origin via the northern LLWBCs (Figures 5b and 5c). The Nd concentrations are relatively high, except at station EUC-Fe 28 (2.5 pmol kg^{-1}), located downstream from the Sepik River (Figure 5d).
3. In the equatorial band, ε_{Nd} decreases as the TW flows eastward in the EUC, more particularly for the 2°S stations. For these 2°S stations, oxygen content and salinity both increase as ε_{Nd} decreases eastward (Figures 5b and 5c). In contrast, salinity and oxygen concentrations at the 2°N stations decrease from 180° to 140°W (EUC-Fe 13 and 1). Along the equator, ε_{Nd}, salinity and oxygen values seem to be more constant. Nd concentrations do not display any gradient along the southern equatorial stations, and overall these stations are characterized by relatively low values (3.3–3.6 pmol kg^{-1}; Figure 5d). Equatorial stations exhibit the highest Nd concentrations of TW (5.1–5.4 pmol kg^{-1}).

4.1.2.2. Central Waters

[29] The ε_{Nd} values of CW range from -2.7 to -1.2 (Figure 6a). The most radiogenic CW was found at station 28, downstream from the Sepik River. Surprisingly, every other ε_{Nd} value for CW collected west of 180° is at least 0.8 unit lower (mean: $\varepsilon_{Nd} = -2.4 \pm 0.1$; $n = 7$). At 140°W, the average ε_{Nd} is -1.7 ± 0.1 ($n = 3$), which is more radiogenic than that in the west. This ε_{Nd} distribution contrasts with those of SW and TW, whose central equatorial samples were characterized by less radiogenic values than those close to the western coasts. The saltiest CW were found at the 2°S stations (>35 west of 180°; Figure 6b) whereas waters fresher than 35 were found in the southern subtropical gyre and at the 2°N and 0° stations. Oxygen concentrations display the most heterogeneous distribution (Figure 6c). The most oxygenated CW ($O_2 = 135$–$200\ \mu\mathrm{mol\,kg^{-1}}$) are found

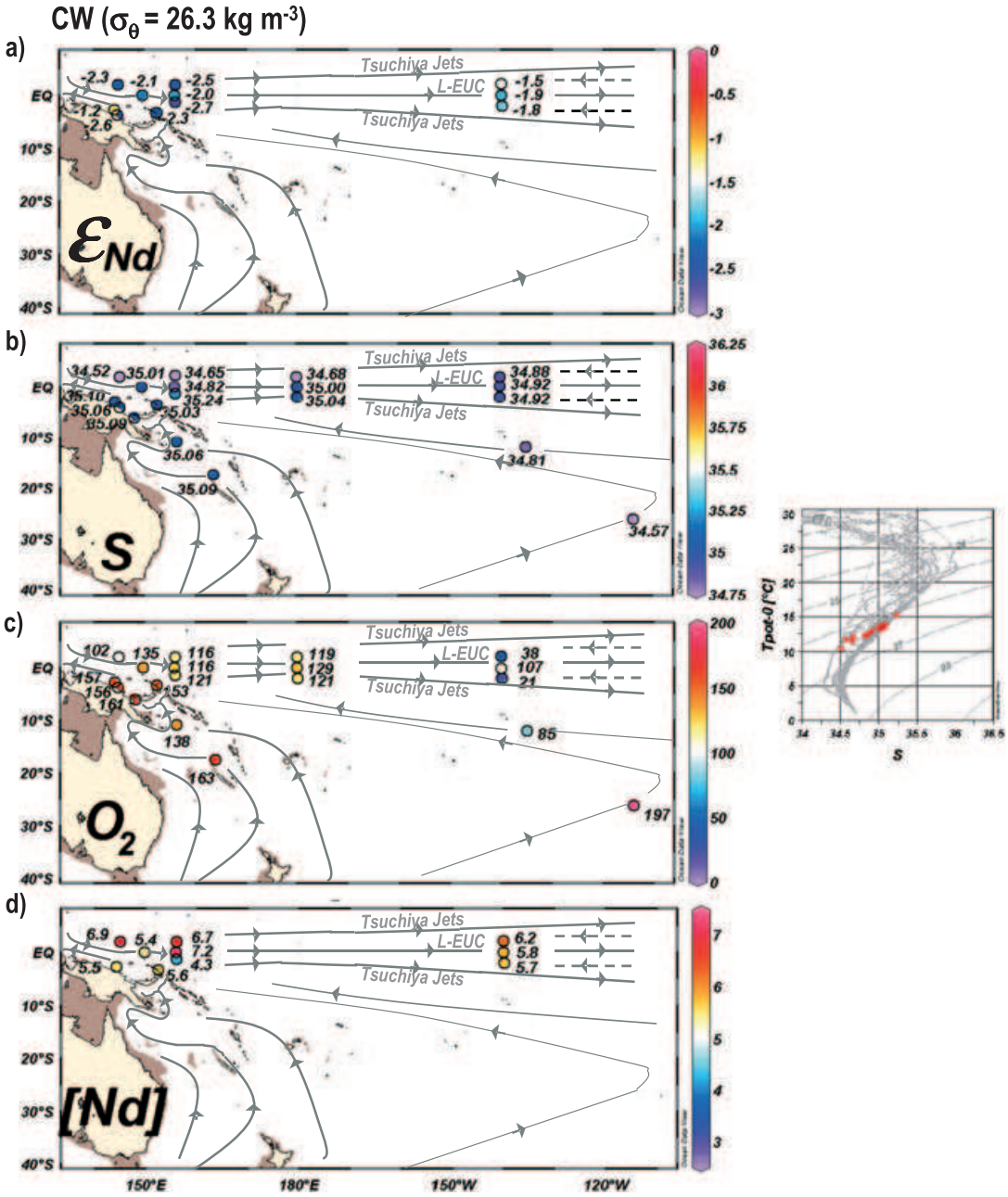

Figure 6. As Figure 5, for Central Waters ($\bar{\sigma}_\theta = 26.3\,\mathrm{kg\,m^{-3}}$). The bathymetry shallower than 250 m is colored in brown.

at station GYR (*C. Jeandel et al.,* [2013]) and in the south western boundary area. In the equatorial band, the O_2 content ranges from 100 to 135 μmol kg^{-1} west of 180°. In contrast, at 140°W, the 2°N and 2°S stations exhibit very low O_2 concentrations at the density of WSPCW (<50 μmol kg^{-1}) whereas the 0° station is still well oxygenated. Nd concentrations of CW are spatially almost constant, averaging 5.9 ± 0.3 pmol kg^{-1} (n = 10; Figure 6d).

4.1.3. Subantarctic Mode Water

[30] Twelve samples were collected at this density level for the measurement of ε_{Nd}. As for CW, SAMW is less radiogenic in the western boundary area, west of 160°E (ε_{Nd} = [−3.3; −2.2]), than in the central equatorial Pacific, at 140°W (ε_{Nd} = [−1.9; −1.4]; Figure 7a). Salinity increases slightly between the subtropical gyre (station GYR) and the Bismarck Sea, via the Coral and Solomon Seas (Figure 7b). These SAMWs exhibit high O_2 concentrations, decreasing slightly from 222 μmol kg^{-1} in the subtropics to 170 μmol kg^{-1} in the Bismarck Sea (Figure 7c). The saltiest and less oxygenated SAMWs are found in the equatorial band ($\bar{S}$ = 34.7, 10 < O_2 < 100 μmol kg^{-1}), with oxygen falling to 10–35 μmol kg^{-1} at 140°W. Nd concentrations range from 4.9 pmol kg^{-1} at 180°-2°S to 8.4 pmol kg^{-1} downstream of the Sepik River, at station 28 (Figure 7d). Although very far from our study area, the recent data of *Carter et al.* [2012] showed that, at its source in the southeast Pacific, subducting SAMW is tagged by much less radiogenic value (ε_{Nd} ~ −8.6).

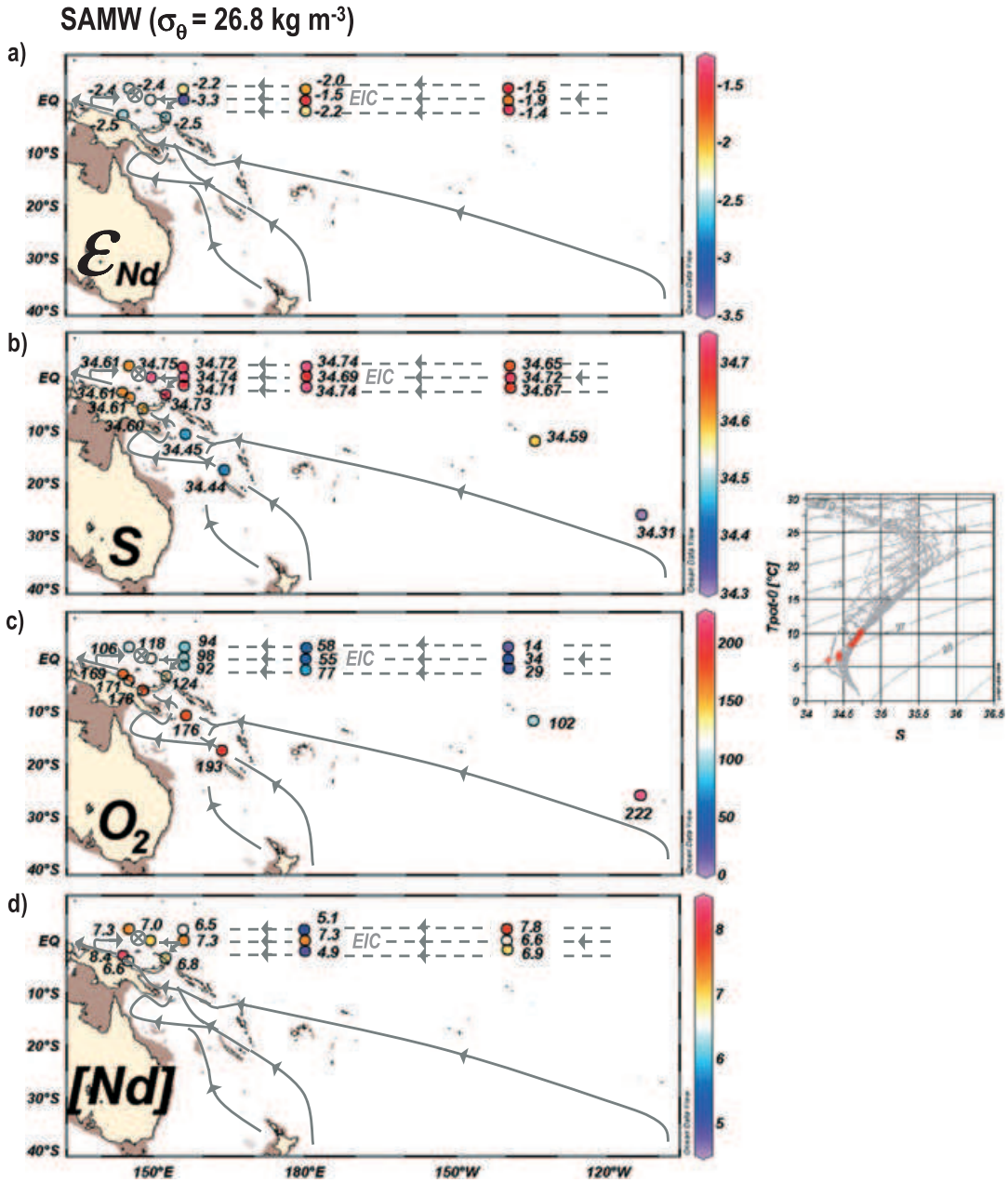

Figure 7. As Figure 5, for waters characterized by $\bar{\sigma}_\theta = 26.8\,\mathrm{kg\,m^{-3}}$. See text for the definition of the different water masses flowing at this density. The bathymetry shallower than 250 m is colored in dark brown, in light brown if shallower than 500 m.

4.1.4. Intermediate Waters

[31] The ε_{Nd} values of IW range from −8.0 at station EqPac to −2.1 at station 28 and at 140°W (Figure 8a). Between the subtropics and 5°S, this parameter increases from −8.0 to −4.0. This area corresponds to the most oxygenated and freshest IW of our study, located at station GYR and within the Coral and Solomon Seas (Figures 8b and 8c). North of 5°S, IW exhibits a rather constant ε_{Nd} (mean: $\varepsilon_{Nd} = -2.4 \pm 0.2$; $n = 11$). In contrast, the oxygen content of IW drops to low values along the equator ($70 < O_2 < 110\ \mu\mathrm{mol\,kg^{-1}}$), whereas its salinity is quasi-homogeneous around 34.54. These parameter values are in good agreement with those given for the EqPIW by *Bostock et al*. [2010]. Nd concentrations are spatially almost constant, varying from 7.0 pmol kg^{-1} at 180° to 9.7 pmol kg^{-1} within the Coral Sea, with slightly higher concentrations from the Coral Sea to Bismarck Sea than in the equatorial band (Figure 8d).

4.1.5. Bottom and Deep Waters

[32] The ε_{Nd} values of UCDW range from −3.7 in the southern subtropical gyre to −0.7 downstream of the Sepik River (Figure 9a). At each station, UCDW is more radiogenic than the IW just above. This water mass is relatively well oxygenated at station GYR and in the Coral and Solomon Seas (~150 μmol kg^{-1}) and is less oxygenated as it flows along the coasts of PNG and New Ireland (120 μmol kg^{-1}).

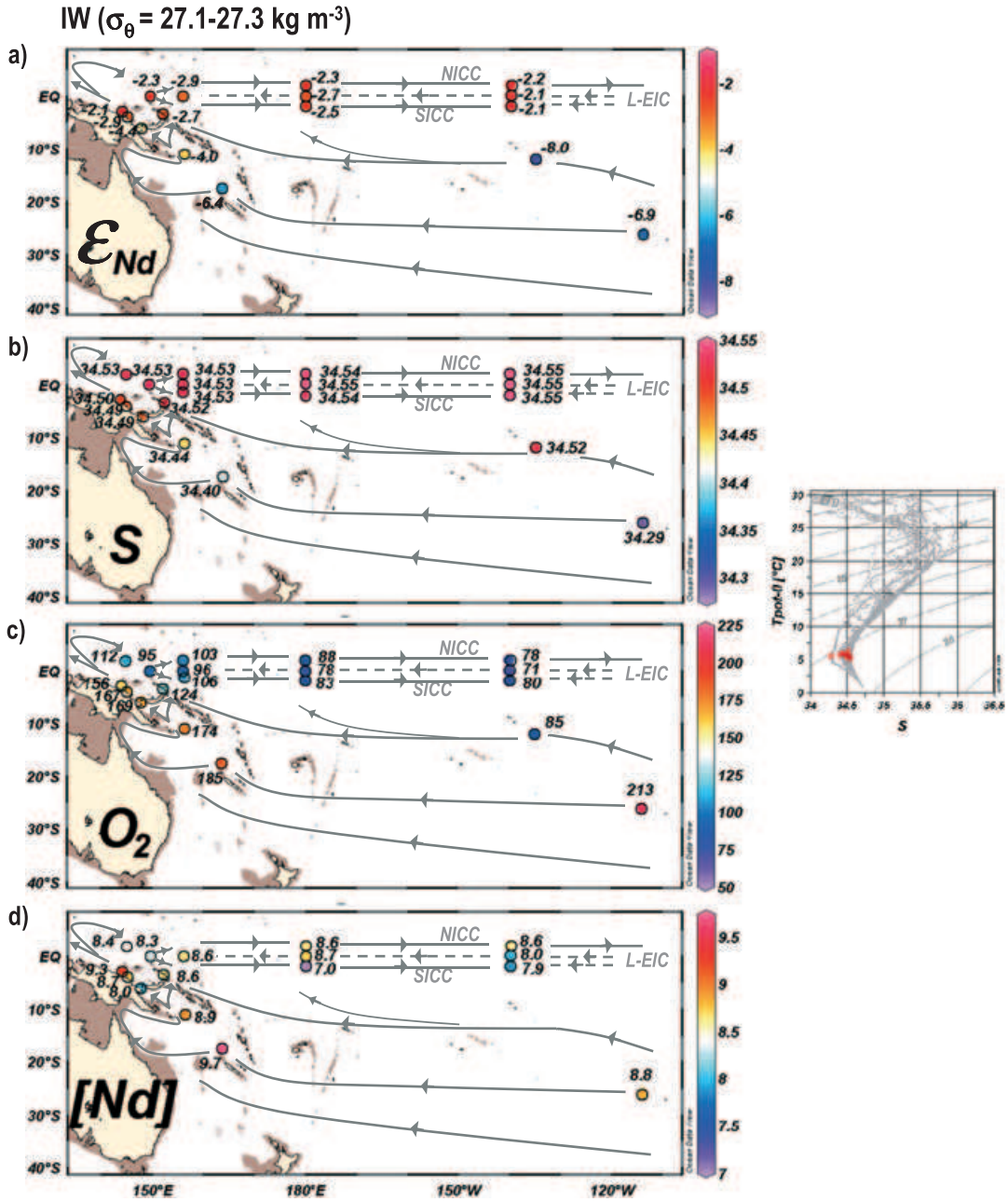

Figure 8. As Figure 5, for Intermediate Waters (σ_θ = 27.1–27.3 kg m^{-3}). The bathymetry shallower than 750 m is colored in dark brown, in light brown if shallower than 1000 m.

[33] Finally, oxygenated LCDW was collected at one station (EUC-Fe 14, 180°-0°; Tables 1 and 2) and was characterized by $\varepsilon_{Nd} = -7.2$.

4.2. Rare Earth Element Patterns

[34] The REE concentrations are compiled in Table 2. REE fractionation relative to the continental source is identified by normalizing the REE concentrations to the average value of Post-Archean Australian Shale (PAAS) [*McLennan*, 1989]. As an example, the PAAS-normalized REE pattern is presented in Figure 10a for station 25. It shows the main characteristics of dissolved marine REE patterns: a negative Ce anomaly, increasing with depth, and a marked enrichment in heavy REE (HREE) [*De Baar et al*., 1985; *Elderfield*, 1988; *Tachikawa et al*., 1999]. Interestingly, significant positive Eu and Gd anomalies characterize most of the patterns, as well as a slight negative Yb anomaly. All the stations at which samples have been measured using the desolvator displayed similar patterns, even at depth. Other stations exhibit comparable patterns, although marked by lesser Eu anomalies, which could reflect an overcorrection of the oxide interferences (see section 2).

[35] Following the approach of *Sholkovitz et al*. [1999], we chose to normalize our REE concentrations to those of the same water mass — taken as reference — at a station located in the center of the Coral Sea (station SA-7 of

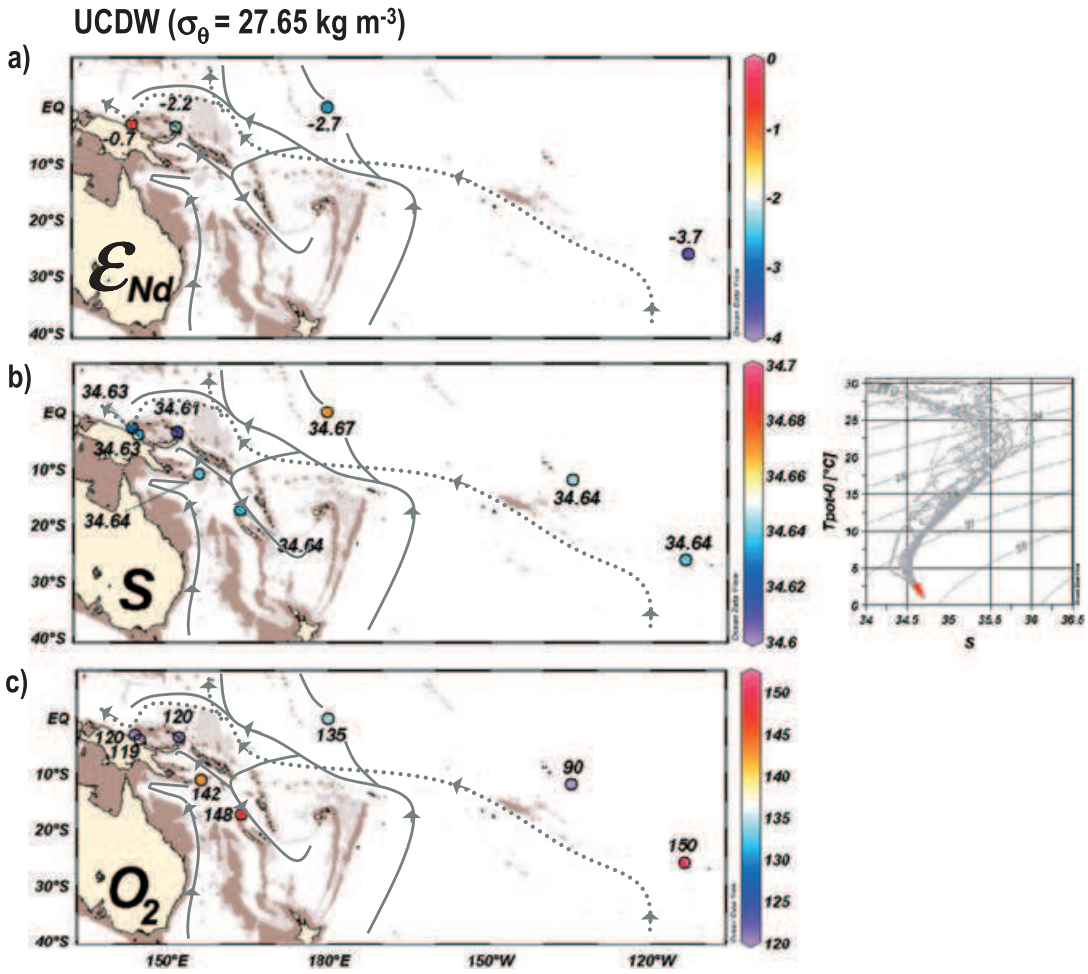

Figure 9. As Figure 5, Upper Circumpolar Deep Waters ($\overline{\sigma_\theta}$ = 27.65 kg m^{-3}). The bathymetry shallower than 1500 m is colored in dark brown, in light brown if shallower than 2500 m. Filled arrows and dotted arrows represent the UCDW pathways described by *Sokolov and Rintoul* [2000] and by *Kawabe and Fujio* [2010], respectively. Nd concentrations were not measured at this depth for most of the stations and, consequently, are not figured.

Zhang and Nozaki [1996]). Indeed, Nd and Eu concentrations of SA-7 are the lowest of the studied area, except for the surface waters of station GYR (Figures 11b and 11c; *C. Jeandel et al.,* [2013]). We use this "reference" to determine qualitatively the REE pattern evolution of the water masses from the Coral Sea, that is, upstream from the Papua New Guinea area, previously suggested as a crucial area determining the geochemical character of Pacific equatorial water masses [*Lacan and Jeandel*, 2001; *Slemons et al*., 2010]. This also facilitates a direct comparison with previously published results [*Zhang and Nozaki*, 1996; *Sholkovitz et al*., 1999]. SA-7-normalized REE patterns of thermocline and deep waters are shown in Figure 10. SA-7-normalized Ce concentrations are not presented here because *Zhang and Nozaki* [1996] expressed some doubts about their Ce data. Nevertheless, the vertical distribution of our Ce results is presented in Figure 11. Because REE results of stations GYR, 28, 22, and 14 had significant interferences with BaO that particularly affected Eu peaks, we do not present the normalized-Eu for these stations in Figures 10b–10d.

[36] Normalization to SA-7 allows the identification of any qualitative changes that the REE content of the studied waters has undergone — enrichment, scavenging, precipitation — between this "Coral Sea reference" and stations analyzed in this study. A clear positive Eu anomaly characterizes each water mass, together with systematic, although less marked, anomalies in Eu's neighbors, Sm and Gd (Figure 10). The fact that three middle REEs (MREEs) are enriched allows the elimination of an artifact hypothesis that the striking positive Eu anomaly observed in our data could be due to an underestimation of Zhang and Nozaki's [1996] Eu concentrations. In addition we also normalized our data to the REE data of station TPS24 271-1 from *Piepgras and Jacobsen* [1992]. These authors' analyses used the isotopic dilution method on each individual poly-isotopic REE and were measured on a TIMS, avoiding any interference problem. This normalization (not shown) confirmed the occurrence of a positive Eu anomaly in our samples. Furthermore, our data are consistent with the preferential release of MREE already observed during reaction between terrigenous particles and seawater, a phenomenon that could be due to the

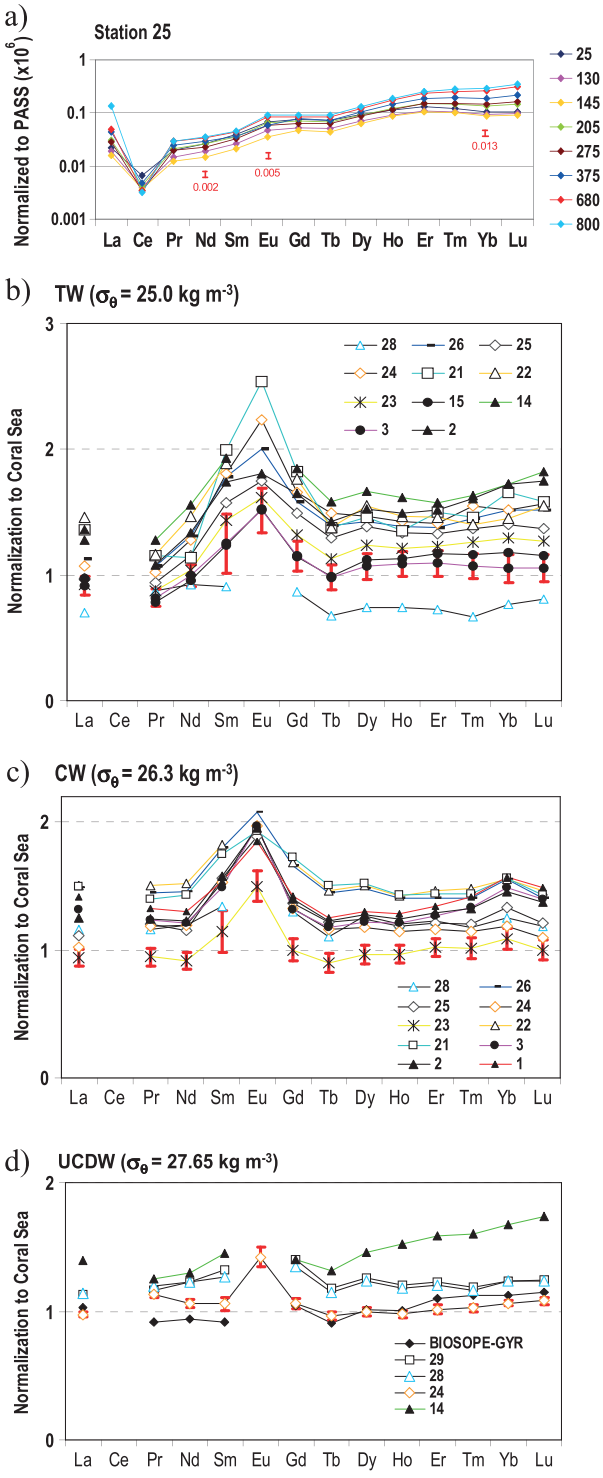

Figure 10. REE pattern for (a) station 25 normalized to PAAS (logarithmic scale) and REE patterns for (b) Tropical Waters, (c) Central Waters, and (d) deep waters of our study normalized to REE patterns of TW, CW, and deep waters obtained at SA-7 [*Zhang and Nozaki*, 1996]. The depths selected at SA-7 as references for TW, CW, and UCDW are 149 m, 298 m, and 1980 m, respectively. Mean error bars are shown in red.

electronic configurations of their atoms [*Byrne and Sholkovitz*, 1996; *Sholkovitz et al.*, 1999]. Surprisingly enough, this anomaly is well preserved along the water mass pathways, particularly for the CW, from the western coasts of the basin to the central equatorial Pacific (Figure 10b).

[37] The surface waters (SW) displaying the highest REE contents are found at station 28, just north of the Sepik River (Figures 11a–11c). In terms of ε_{Nd}, they are also the most radiogenic waters of our study (Figure 11d). The surface REE concentrations decrease away from the western boundary regions. Beneath the surface, we observe a concentration minimum in Nd and Eu for most of TW studied here. Contrasting with SW, the lowest REE concentrations are found at station 28 for Tropical Waters (TW; Table 2 and Figures 11a and 11b). The TW highest in REE were collected at stations 24, 26, and 14, whereas the most concentrated Central Waters (CW) were collected at stations 24, 25, 26, and 21. At densities higher than that of CW, Eu and Nd concentrations display vertical profiles that are similar from one station to another, increasing with depth. In contrast, Ce concentrations are relatively heterogeneous in these deeper layers, showing high concentrations for IW and UCDW at stations GYR, 28, and 24 (Figure 11a).

5. Discussion

[38] Tropical Pacific seawaters are characterized by a mean $\varepsilon_{Nd} = -2.0 \pm 0.2$ ($n = 117$), including GYR, EqPac, FLUSEC, and EUC-Fe stations (see grey band in Figure 11d). The seawater samples measured in this study are among the most radiogenic observed in any part of the ocean so far [see Figure 5 of *Lacan et al.*, 2012], the most radiogenic of our study being SW close to the western coast (see Table 1 and Figure 4a). Despite these relatively homogeneous ε_{Nd} values, there are significant deviations from this average that are discussed below. Because changes in the isotopic signatures of water masses are strongly related to those of the nearby coasts, we propose first to review the isotopic and REE characteristics of the potential sources of elements in this area.

5.1. Characterization of the Sources

[39] Figure 12 presents ε_{Nd} and REE data for rocks and sediments extracted from the largest geochemical data set, EarthChem (http://www.earthchem.org). Most of the continental and oceanic samples of our area are very radiogenic, characterized by ε_{Nd} greater than +5 (Figure 12a). On the oceanic side, the most radiogenic fields are the mid-Pacific ridge, the Bismarck Sea and the Solomon Sea. On the continental one, the most radiogenic fields are Vanuatu, Galapagos, and Costa Rica (Figure 12a). On the contrary, the islands surrounding the Banda Sea (area no. 1) and the coasts of Peru (no. 14) and of Mexico (no. 9) exhibit the least radiogenic continental values ($\overline{\varepsilon_{Nd}} = -7.3 \pm 8.8$, $\overline{\varepsilon_{Nd}} = -5.5 \pm 5.8$, and $\overline{\varepsilon_{Nd}} = +2.8 \pm 9.7$, respectively).

[40] Figure 12b displays the average REE patterns of outcropping samples for areas numbered from 1 to 14, normalized to PAAS (left panel) and to surface waters of the Coral Sea (0 m depth sample of SA-7; right panel). Except for areas 1, 9, and 14, the REE patterns normalized to PAAS show that light REE (LREE) are significantly depleted compared to HREE and display a Eu maximum. For areas 1, 9,

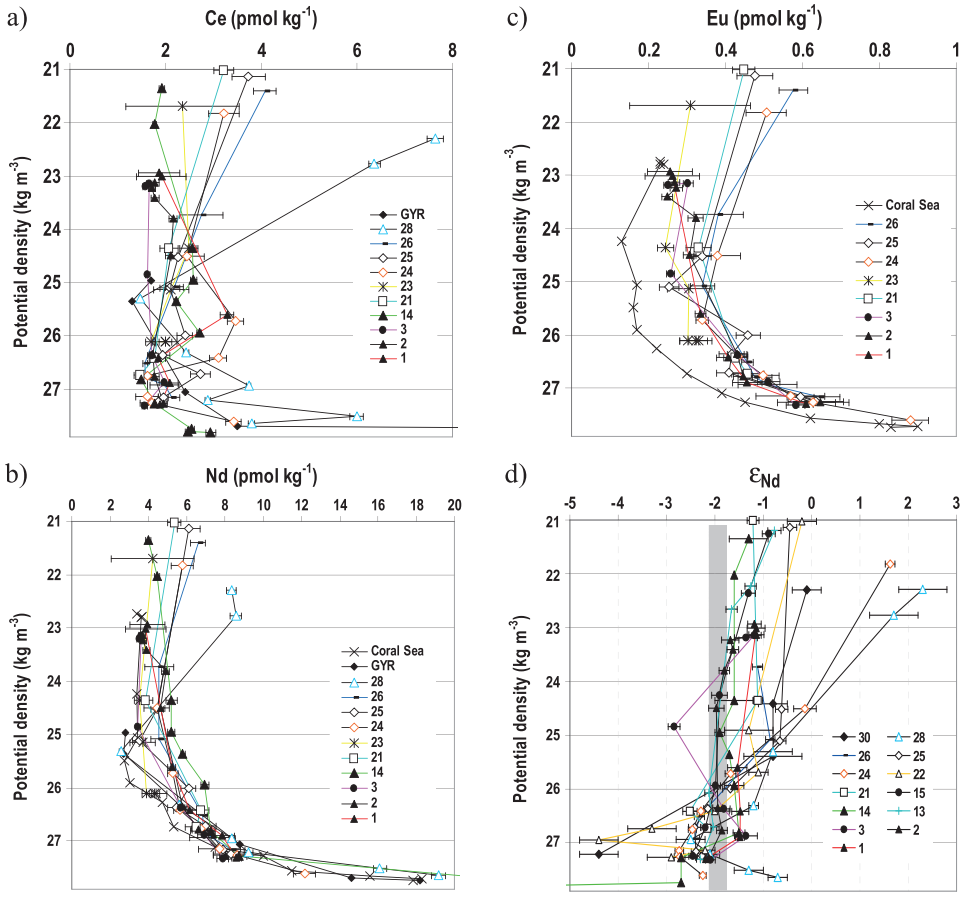

Figure 11. (a) Ce, (b) Nd, and (c) Eu concentrations (pmol kg^{-1}) as a function of potential density (kg m^{-3}). The Coral Sea vertical profiles correspond to *Zhang and Nozaki*'s [1996] data. (d) Vertical profiles of ε_{Nd}, with associated error bars. The grey band represents the mean ε_{Nd} value of the seawater samples studied here.

and 14 — and also samples with the less radiogenic Nd as presented just above — the Eu maximum is still marked but the LREE depletion is much weaker. The average REE patterns for Peru even show the opposite pattern, with depleted HREE compared to LREE. As the average composition of the Earth's crust is mostly granitic, the flat REE patterns with PAAS-normalized values near or below unity that characterize areas 1, 9 and 14 reflect a crustal composition dominated by granites whereas the inclined REE pattern of other areas reflect a crustal composition mostly made up of basalts [*Sun and McDonough*, 1989].

[41] When normalized to surface waters of station SA-7, the REE data of these rock samples display significant positive Sm and Eu anomalies (Figure 12b). Again, areas 1, 9 and 14 show different patterns, with no positive Sm-Eu anomaly and LREE enrichment characterized by a decreasing slope from Pr to Er.

5.2. Modification of Seawater ε_{Nd} by Interaction With Ocean Margins and Bottom

[42] From results extracted from Figures 4 to 12, we have identified different sources that could impact the ε_{Nd} of water masses along their pathways. Most are identified in Figure 1.

5.2.1. Fiji, Tonga and Vanuatu

[43] The TW of southern hemisphere origin is formed in the HSEA, in the longitude and latitude ranges of 105°W-145°W and 10°-24°S, respectively (hatched area of Figure 1) [*Tsuchiya et al.*, 1989]. TW subducting in the vicinity of station GYR is conveyed by the anticyclonic subtropical gyre westward toward Australia [Figure 8.6 of *Tomczak and Godfrey*, 2003]. Then, these TW bifurcate northward toward the Coral Sea [*Qu and Lindstrom*, 2002]. Consequently, station GYR can reasonably be considered as a source of TW of the Coral and Solomon Seas stations (FLUSEC 43 and FLUSEC 22; Figure 5). A Lagrangian simulation is currently underway, of which the first results confirm this hypothesis. Interestingly, the ε_{Nd} values are significantly different at these three stations: TW at station GYR are the least radiogenic ($\varepsilon_{Nd} = -2.7$), TW flowing at station FLUSEC 43 are more radiogenic ($\varepsilon_{Nd} = -1.8$) and the most radiogenic TW is found at FLUSEC 22 ($\varepsilon_{Nd} = -0.3$). These results suggest that TW has encountered radiogenic sources between GYR and the Coral Sea. Rock samples collected on Samoa are characterized by $\overline{\varepsilon_{Nd}} = +2.0 \pm 2.0$ ($n = 200$; EarthChem database). Similarly, $\overline{\varepsilon_{Nd}} = +7.5 \pm 1.5$ ($n = 39$) at Fiji, $\overline{\varepsilon_{Nd}} = +8.4 \pm 1.1$ ($n = 17$) at Tonga, and $\overline{\varepsilon_{Nd}} = +7.2 \pm 3.5$ ($n = 86$) at Vanuatu. All these radiogenic lithogenic margins represent potential sources for TW flowing in the vicinity of their coasts. Three hypotheses could explain slightly less radiogenic TW observed at FLUSEC 43 compared to FLUSEC 22: (i) TW flowing at FLUSEC 43 are transported at higher latitude than those collected at

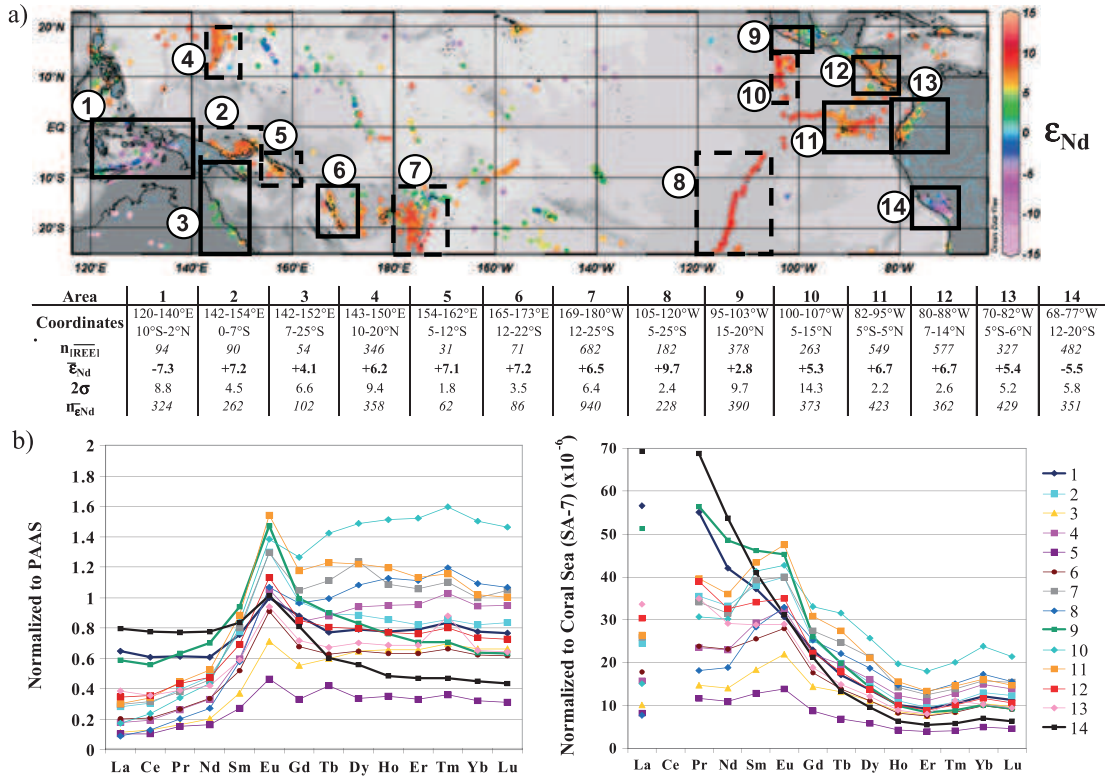

Area	1	2	3	4	5	6	7	8	9	10	11	12	13	14
Coordinates	120-140°E 10°S-2°N	142-154°E 0-7°S	142-152°E 7-25°S	143-150°E 10-20°N	154-162°E 5-12°S	165-173°E 12-22°S	169-180°W 12-25°S	105-120°W 5-25°S	95-103°W 15-20°N	100-107°W 5-15°N	82-95°W 5°S-5°N	80-88°W 7-14°N	70-82°W 5°S-6°N	68-77°W 12-20°S
$n_{[REE]}$	*94*	*90*	*54*	*346*	*31*	*71*	*682*	*182*	*378*	*263*	*549*	*577*	*327*	*482*
$\overline{\varepsilon_{Nd}}$	**-7.3**	**+7.2**	**+4.1**	**+6.2**	**+7.1**	**+7.2**	**+6.5**	**+9.7**	**+2.8**	**+5.3**	**+6.7**	**+6.7**	**+5.4**	**-5.5**
2σ	8.8	4.5	6.6	9.4	1.8	3.5	6.4	2.4	9.7	14.3	2.2	2.6	5.2	5.8
$n_{\varepsilon Nd}$	*324*	*262*	*102*	*358*	*62*	*86*	*940*	*228*	*390*	*373*	*423*	*362*	*429*	*351*

Figure 12. (a) ε_{Nd} of samples of rocks and sediments extracted from the geochemical data set EarthChem. The table, for each area numbered from 1 to 14, gives the associated ε_{Nd} and its 2σ, $n_{\varepsilon Nd}$, the number of samples from which the average ε_{Nd} is obtained, and $n_{[REE]}$, the number of samples on which the average REE patterns shown in Figure 12b are based. Dashed (continuous) black rectangle delimiting an area means that most of the samples for which data are compiled in that area are sediments (rocks). (b) PAAS-normalized (left) and SA-7-normalized (right) REE patterns of rock and sediment samples, also extracted from EarthChem.

FLUSEC 22 and may encounter fewer islands on their pathway than the latter; (ii) FLUSEC 22 is located in an area of recirculating eddies [*Gasparin et al.*, 2012] and the more radiogenic isotopic composition of TW could be due to their long residence time in the Solomon Sea flowing past radiogenic New Ireland and Solomon Island margins; and (iii) TW flowing at FLUSEC 43 may not only originate from the HSEA but also come from a less radiogenic southwestern origin, maybe close to Tasman Sea. This last hypothesis is consistent with *Wyrtki*'s [1962] scheme, specifically with the salinity data and oxygen properties. However, this issue is beyond the scope of this study and will be discussed in a further paper.

[44] The ε_{Nd} values and Nd concentration variations affecting IW suggest that their chemical enrichment is less important than that of TW during their transit from the gyre toward the Coral Sea. One explanation could be that IW reach the Coral Sea via a more southeast-northwest direction compared to TW and may flow past fewer, if any, islands before flowing past New Caledonia.

5.2.2. Papua New Guinea (PNG), Solomon Islands, and New Ireland Areas

[45] An important increase of ε_{Nd} value is observed for TW and IW between the southeastern entrance of the Coral Sea, south of Vanuatu (station FLUSEC 43), and north of the Solomon Sea (stations 30 and 24). Geological samples collected on the northeast coast of Australia, on the southeast coast of PNG, and on the western side of Solomon Sea are characterized by an average value $\overline{\varepsilon_{Nd}} = +4.1 \pm 6.6$ ($n = 102$; Figure 12a). The ε_{Nd} increase of IW is coupled to a [Nd] decrease. This feature implies that during its transit in Coral and Solomon Seas, the IW is more depleted of its dissolved Nd — likely by scavenging onto particles — than it is enriched by release from the solid phases into the dissolved pool. However, the sparseness of our data does not allow us to identify the locations and causes of this scavenging.

[46] Changes toward more radiogenic ε_{Nd} values are observed for SW, TW, IW, and UCDW as they flow along the margins of PNG and New Ireland (NI; Figures 5a, 6a, 8a, and 9a). It is also in this area that these water masses exhibit the most radiogenic values, particularly at stations 28 and 24. Our ε_{Nd} results are in good agreement with SW values measured at station EQ-1, very close to stations 25 and 22 ($\varepsilon_{Nd} = +0.2$) [*Tazoe et al.*, 2011]. Sediment samples measured in these areas are characterized by mean ε_{Nd} values higher than +7 (Figure 12a). The remarkable increase of ε_{Nd} value for SW between stations 29 and 28 could first be attributed to the Sepik River discharge (Figure 4a). However, Nd isotopic measurements of unfiltered Sepik river water revealed less radiogenic values ($\varepsilon_{Nd} = -3.1$; Sholkovitz, personal communication, 2000) than the sediment margins, values close to that of sediments collected at

80 m depth just north of the Sepik estuary ($\varepsilon_{Nd} = -2.3$). These results preclude the hypothesis of a direct imprint of the Sepik River. On the contrary, a very radiogenic value was measured for the Rabaul Volcano ashes ($\varepsilon_{Nd} = +7.9$), located close to St. George's Channel, in New Britain (Figure 1). Considering the activity of numerous regional volcanoes at the time of the cruise (http://www.volcano.si.edu/world/find_eruptions.cfm), particularly the Manam Volcano located southeast of station 28, and that the winds mostly blow from the southeast during the cruise season [*Ueki et al*., 2003], the increase of SW ε_{Nd} value between stations 29 and 28 could rather be explained by supply of volcanic dust at the sea surface, either by direct ash deposition and dissolution or by streaming along the volcano's slope. Similarly, the radiogenic value found for SW along the New Ireland coast ($\varepsilon_{Nd} = +1.6$) may be the imprint of supply from active volcanoes such as Bagana (Bougainville Islands), Rabaul or Ulawun (New Britain) [*Slemons et al*., 2010].

[47] Reasons for the surprisingly low Nd concentration found within TW at station 28 are unclear. The hypothesis of strong removal of dissolved Nd due to the significant concentration of particles from river discharge was explored, but is not consistent with relatively high Nd concentrations in overlying SW and underlying CW. Local scavenging due to an Intermediate Nepheloid Layer is the most reasonable process that could be invoked, consistent with the down-canyon transport observed by *Kineke et al*. [2000] near the Sepik River mouth.

[48] The observed ε_{Nd} signature changes in water masses flowing at levels as deep as 2000 m preclude an impact of atmospheric and river discharge only and strongly suggest release of Nd from the radiogenic margin material as the water masses flow past it. The basaltic margins of the region have already been suggested to be major sources of lithogenic material for the water masses feeding the equatorial central Pacific [*Lacan and Jeandel*, 2001; *Slemons et al*., 2010; *Tazoe et al*., 2011]. Our study confirms this hypothesis and goes further, showing that every water mass from surface to bottom is influenced by this release of radiogenic Nd from local sediments. Notably, the IWs flowing from station EqPac to station 24 — a pathway that is in agreement with respective parameters S and O_2 (Figures 8b and 7c) — undergo a very significant increase in ε_{Nd}, from $\varepsilon_{Nd} = -8.0$ to $\varepsilon_{Nd} = -2.7$, possibly due to margin dissolution along the Solomon Islands and New Ireland.

5.2.3. Kiribati

[49] Data characterizing SW conveyed westward along 0° by the SEC reveal a significant increase in ε_{Nd} values and Nd concentrations between 180° and 156°E (Figures 4a and 4d, respectively). *Messié et al*. [2006] observed a huge bloom of phytoplankton just west of the Gilbert Islands, the main part of Kiribati Islands (Figure 1; coordinates: 2.5°S-3.5°N; 172°E-176°E). The authors suggested that the bloom was due to EUC shoaling enhanced by the island obstacle, reaching the euphotic zone and implying a sudden input of iron, available for photosynthesis. However, the comparison of TW and SW characteristics at 156°E-0° precludes any influence of upwelled TW at these sites: TW is less radiogenic ($\varepsilon_{Nd} = -1.3$), saltier (S = 35.20), and less oxygenated ($O_2 = 126\ \mu mol\ kg^{-1}$) than SW (Figure 5). We rather suggest two other explanations. On the one hand, in the western Pacific, surface currents are weak and occasionally eastward [*Reverdin et al*., 1994]. In such case, the ε_{Nd} differences between 156°E and 180° could be explained by eastward advection of radiogenic SW from the coastal areas of PNG and New Ireland. On the other hand, if the convergence zone of surface currents was west of 156°E, the ε_{Nd} differences between 156°E and 180° could be explained by a release of radiogenic ε_{Nd} from Gilbert Islands margin material within SW during the westward advection of the SEC, which would also lead to increased supplies of trace metals such as iron that could stimulate the phytoplankton bloom. *Zhang et al*. [2008] suggested a similar mechanism to explain the natural fertilization of the Kerguelen Plateau. This hypothesis is consistent with the observation that the ε_{Nd} signature of intraplate volcanoes measured in this archipelago is radiogenic (Figure 12a) [*Konter et al*., 2008]. Just before the cruise period, westerly winds were blowing and could have implied weak eastward currents (not shown). However, ADCP data showed eastward surface currents only west of 156°E (stations 24–26); at 156°E and further east, surface currents were westward, unless for station 13. Therefore, the more likely explanation for this ε_{Nd} discrepancy is the Kiribati margin contribution.

5.2.4. Eastern Equatorial Pacific Margins and Galapagos

[50] Surprisingly, the seawater collected at $\sigma_\theta = 26.3\ kg\ m^{-3}$ (average depth: 275 m) is more radiogenic at 2°N-140°W ($\varepsilon_{Nd} = -1.5$) and 2°S-140°W ($\varepsilon_{Nd} = -1.8$) than at 156°E although the stations are located in the central equatorial Pacific, far from potential lithogenic enrichment (Figures 6a and 12a). Furthermore, both samples have a very low dissolved oxygen concentration compared with the equatorial station 2 or those at 156°E (Figure 6c). Similarly, the seawater collected at $\sigma_\theta = 26.8\ kg\ m^{-3}$ is more radiogenic at the six stations of the central equatorial Pacific than those located close to the PNG and New Ireland coasts (Figure 7a). Again, differences in dissolved oxygen contents are observed, the "central" water being poorly oxygenated compared to the "western" waters ($O_2 = 0$–$75\ \mu mol\ kg^{-1}$ and $O_2 = 90$–$200\ \mu mol\ kg^{-1}$, respectively; Figure 7c). From these results, we suggest that radiogenic and poorly oxygenated waters in the central equatorial Pacific at these two densities were collected within westward currents: that is, they might originate from the eastern equatorial Pacific. ADCP data agree with this circulation for every sample except for the SAMW collected at station 3, where they show a weak eastward current (not shown). Actually, *Rowe et al*. [2000] showed that the cores of the Tsuchiya Jets, which carry the $26.3\ kg\ m^{-3}$ waters, diverge and shoal between 2°N/S at 170°E and 6°N/S at 125°W. Thus, at 140°W-2°N/S and $\sigma_\theta = 26.3\ kg\ m^{-1}$, the seawater samples were likely collected within westward currents (SEC or EIC). These waters might result from a mixing of oxygenated waters advected eastward by Intermediate Countercurrents (ICCs) with poorly oxygenated waters advected westward from the oxygen minimum zone (OMZ) by the EIC. This mixing likely occurs along the equator, as indicated by interleaving layers identified by oxygen fingering at 156°E and at 180° (Figure 3) [*Stramma et al*., 2010]. *Grasse et al*. [2012], at 3°35′S-85°50′W, measured an almost anoxic water mass at $\sigma_\theta = 26.87\ kg\ m^{-3}$ that is associated with $\varepsilon_{Nd} = -2.8 \pm 0.1$. They also measured several water samples in the σ_θ range 26.17–$26.33\ kg\ m^{-3}$ with a mean $\overline{\varepsilon_{Nd}} = -2.5 \pm 0.3$ ($n = 5$). These waters are likely advected

westward by the EIC from the eastern equatorial Pacific OMZ and their contact with radiogenic islands such as Galapagos results in an increase of ε_{Nd} along their route to 140°W (Figure 12a). Similarly, IW collected at 140°W could partly come from the eastern Pacific, advected westward by the lower EIC. Our ε_{Nd} values are consistent with a possible mixing of west Pacific IW, oxygenated and less radiogenic, and east Pacific IW, poorly oxygenated and more radiogenic. *Grasse et al*. [2012] found IW of $\varepsilon_{Nd} = -1.6 \pm 0.4$ at 1°40′N-85°50′W.

5.2.5. Bottom Sediments

[51] *Piepgras and Wasserburg* [1982] observed an LCDW less radiogenic ($\varepsilon_{Nd} = -8.1 \pm 0.6$) at 20°00′S-159°59′W than the one we collected at station 14 ($\varepsilon_{Nd} = -7.2 \pm 0.3$). Once again, this change could reflect enrichment along its route from the tropics to the equator. As LCDW flows just above the ocean floor, this may reflect an impact of Nd release from resuspended sediments. The ε_{Nd} values that *Aplin et al*. [1986/1987] measured in the central tropical south Pacific, $\varepsilon_{Nd} = -6.9$ in Fe-Mn encrustations at 4700 m and $\varepsilon_{Nd} = -6.5$ in nodules at 5170 m also argue for this hypothesis. Close sediment ε_{Nd} values were also observed by *Horikawa et al*. [2011] in core-top fossil fish teeth/debris at 175.2°E-0° ($\varepsilon_{Nd} = -4.89$, 4881 m) and at 170°E-4.9°S ($\varepsilon_{Nd} = -5.42$, 5386 m). In areas where the bottom depth does not exceed 3000 m, preventing the occurrence of LCDW, it is also observed that UCDW is more radiogenic than overlying IW. ε_{Nd} values observed at stations 24 ($\varepsilon_{Nd} = -2.2$ vs $\varepsilon_{Nd} = -2.7$) and 28 ($\varepsilon_{Nd} = -0.7$ vs $\varepsilon_{Nd} = -2.1$) illustrate this feature. Once again, our hypothesis is that Nd is released from the sediments deposited on the bottom, followed by diffusion into the water mass.

5.3. The Europium Anomaly

[52] Processes that control the distribution and determine the pattern of dissolved REE in seawater have been studied for years [*Elderfield and Greaves*, 1982; *Byrne and Kim*, 1990, 1993; *Bertram and Elderfield*, 1993; *Alibo and Nozaki*, 1999; *Tachikawa et al*., 1999; *Sholkovitz and Szymczak*, 2000; *Hannigan and Sholkovitz*, 2001; *Akagi et al*., 2011]. Most of these studies argue that dissolved REE distribution is mainly governed by internal processes occurring within the water column. In this view, redox processes and carbonate complexation, together with differential scavenging on carrier phases such as phosphate and organic oxyhydroxides, are the main processes invoked to explain the general shape of seawater REE patterns: a progressive HREE enrichment and the deepening of the Ce anomaly with depth [*De Baar et al*., 1985; *Byrne and Kim*, 1990, 1993; *Lee and Byrne*, 1993]. Phosphate and carbonate mineral phases were also identified as major carriers for REE within equatorial Pacific pelagic sediments [Takebe, 2005]. However, these hypotheses were recently challenged by *Akagi et al*. [2011], who propose that uptake of the REEs in surface water and release at depth may, in the end, be mostly driven by diatoms and the oceanic opal cycle. Moreover, several authors have brought to light the potential importance of riverine supply and sediment remineralization as sources of REE to the open ocean that could significantly impact the shape of the REE pattern [*Sholkovitz et al*., 1994; *Amakawa et al*., 2000; *Nozaki and Alibo*, 2003a, 2003b; *Wang and Yamada*, 2007].

[53] In this study, normalized REE concentrations, either to PAAS or SA-7, exhibit a positive Eu anomaly. This striking feature is observed whatever the water mass density and distance to the coast (Figure 10). It is apparently not affected by the low oxygen contents advected westward from the OMZ in the central Pacific. To this extent, Eu behavior contrasts with Ce, which is preferentially released in anoxic waters [*De Baar et al*., 1985]. This Eu anomaly modifies the shape of the oceanic REE pattern, which becomes marked by an MREE peak. This shape is particularly preserved into the CW (Figure 10c). As for ε_{Nd} value variations, we attribute this new feature characterizing the water masses of the western and central Pacific to the imprint of a lithogenic input. The shape of PAAS- and SA-7-normalized REE patterns of the geological samples plotted in Figure 12b strengthens this hypothesis: almost every area potentially in contact with the studied water masses exhibits similar REE patterns, characterized by a positive Sm-Eu anomaly. Rabaul volcanic ashes also exhibit such positive Sm-Eu anomalies, although they are slightly greater for Sm than for Eu (not shown). Earlier studies which discussed a likely impact of sources to the seawater REE patterns were restricted either to local river discharge or to deep hydrothermal vents. Sholkovitz and his coworkers observed that REE patterns of the Papua New Guinea river water discharges were characterized by an MREE anomaly, in the Sepik as well as the Fly Rivers [*Sholkovitz et al*., 1999; *Sholkovitz and Szymczak*, 2000; *Hannigan and Sholkovitz*, 2001]. These latter authors associated this shape with a preferential dissolution of phosphatic minerals during weathering of continental PNG crust. Other works suggested that hydrothermal fluids of the East Pacific Rise [*Michard et al*., 1983] and in the Manus Basin [*Craddock et al*., 2010] also contribute to such REE patterns, although *Michard et al*. [1983], *Olivarez and Owen* [1989] and *German et al*. [1990] demonstrated that hydrothermal fluids act as a sink for REE, through scavenging onto Fe-Mn precipitates that form when hydrothermal fluids come into contact with seawater.

[54] In the present study, the Eu anomaly is also observed in subsurface, intermediate and deep water masses far from any hydrothermal source, strongly suggesting that these waters experience REE inputs due to submarine weathering of basaltic sediments deposited on the margins. The abundance of potential sources (seamounts and islands) between the subtropics and the equatorial Pacific [*Tomczak and Godfrey*, 2003] can explain the preservation of the positive Eu anomaly in seawater samples collected far from the western boundaries. It may also be due to dissolved/particulate exchange occurring during transit of the water masses. However, we could not clarify this point because we have not yet measured the REE in the solid fraction of our samples. Furthermore, the Eu residence time, estimated to 320–820 years by *Alibo and Nozaki* [1999], is much longer than the residence time of thermocline waters flowing between the subtropics and the equator [*Fukumori et al*., 2004] and is consistent with the preservation of the Eu anomaly. The processes causing REE release to seawater during dissolution of different basalts have been investigated by lab experiment [*Jeandel et al*., 2011; C. R. Pearce et al., The effect of particulate dissolution on the Neodymium (Nd) and rare earth element (REE) composition of seawater, submitted to *Earth and Planetary Science Letters*, 2012). The results show that the kinetics of dissolution

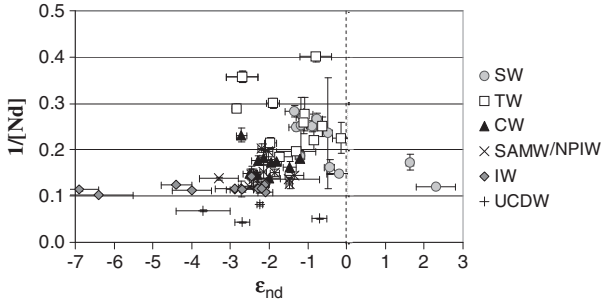

Figure 13. Plot of 1/[Nd] as a function of ε_{Nd}, for the different water masses of the study. A rather constant concentration is observed for waters flowing below the TW (CW, SAMW/NPIW, IW, UCDW).

is rapid (ε_{Nd} equilibrium between seawater and the basaltic source achieved in 1 month), although the controlling processes remain unclear. Therefore, we conclude that the subsurface, intermediate and deep water masses studied here have been imprinted by submarine weathering of sediments deposited on the margins. This process does not preclude the suggestion that surface waters could also be imprinted by exchange with material weathered by rain and wind and carried by rivers. Although on a more local scale, *Zhang et al*. [2008] also concluded that waters of the Kerguelen plateau were imprinted by submarine weathering of the neighboring basaltic islands.

[55] As a whole, seawater REE patterns are not only governed by internal processes, as also suggested recently by *Akagi et al*. [2011]. We show here that weathering of rocks (subaerial as well as submarine) also significantly contributes to the oceanic REE distribution and therefore their patterns. Better constraints on the dissolution kinetics, as well as the other elements that are involved in this weathering, are fundamental issues for future studies to better constrain the fluxes at the land/ocean interface. In the open ocean, far from any sources, the preservation of the positive Eu anomaly is mainly linked to the long residence time of dissolved Eu and highlights the importance of better constraining the fluxes of dissolved/particulate exchange.

[56] Only three studies have so far observed the Eu anomalies in sea water seen here [*Nozaki et al*., 1999; *Amakawa et al*., 2000; *Zhang et al*., 2008]. This could result from two cumulative effects: (1) Eu concentrations are very low and therefore hardly detectable and (2) seawater-dissolved Ba is 1000 times more abundant than Eu, difficult to remove completely during the chemical procedure, and could generate important BaO interferences during the ICP-MS measurement, leading to the risk of an overcorrection of the Eu signal. Thanks to the use of a desolvator (ARIDUS), the observed BaO interferences in our analyses ranged between 0% and 1%. In addition, the blanks were lower than 1% for REE (III) and the mass fractionation is well monitored. All these conditions mean that we are particularly confident in our data.

[57] The ε_{Nd} evolution and the REE patterns suggest inputs due to subaerial and submarine weathering of lithogenic material. However, the Nd concentration variations concomitant with these changes do not argue for dissolution alone, since we do not observe any increase along the water mass pathways (Figures 4d, 5d, 6d, 7d, and 8d). Particularly, Nd concentrations of CW, SAMW, NPIW, IW, and UCDW are relatively constant, consistent with the Nd paradox (Figure 13). The more plausible hypothesis suggested by our results is that scavenging of REE occurred relatively rapidly in the margin area and that, below the TW, the water masses mostly underwent boundary exchange during their ε_{Nd} change [*Tachikawa et al*., 2003; *Lacan and Jeandel*, 2005].

5.4. Evolution Along the Circulation

[58] The preceding section discussed the changes in REE and ε_{Nd} due to exchange with lithogenic material. However, far from any potential source, ε_{Nd} distribution is also constrained by the mixing that water masses undergo along their pathways. As examples, we consider below mixing that likely occurred, and explain ε_{Nd}, S and O_2 parameter variations observed in Figures 4 to 8.

[59] The northern origin of the South Pacific Tropical Water (SPTW) is the HSEA (section 3 and Figure 1). Station EqPac is located in the northwestern part of the core of this HSEA, whereas station GYR is located slightly southeast of this core. Tropical Waters (TW) of these two stations differ in potential temperature, salinity, oxygen and ε_{Nd} (Tables 1 and 2 and Figure 5) and should be considered as different sources of TW. The unradiogenic, salty and oxygenated TW at station EUC-Fe 3 (140°W-2°S) strongly differs from the remaining stations located at its west along the same latitude (2°S). Its ε_{Nd}, S and O_2 values suggest a significant supply from EqPac TW and highlight the interior pathways of TW [see also *Grenier et al*., 2011]. In addition, using the conservative parameters S and θ, we estimated that the water collected at EUC-Fe 3 results from a mixing of 53% of TW from EUC-Fe 15 and 37% of TW from EqPac. The last 11% is CW from EUC-Fe 23 that lightens during its transit within the EUC [*Grenier et al*., 2011]. Using the conservative behavior of Nd isotopes (away from external sources), we assumed that the three considered sources did not undergo any lithogenic enrichment during their transit, and we compared the $\varepsilon_{Nd} = -2.9 \pm 0.5$ associated with these suggested mixing proportions to the one measured at EUC-Fe 3 ($\varepsilon_{Nd} = -2.8$ 0.1). The concordance highlights the quality of the ε_{Nd} tool as tracer of water mass pathways and mixing in remote areas.

[60] The zonal negative (positive) gradient in ε_{Nd} (salt and oxygen contents) observed for stations distributed along 2°S from 156°E to 140°W (EUC-Fe 23, 15 and 3) suggests an increasing proportion of open ocean supply from the EqPac area as the TW flows eastward within the EUC (see arrows indicating these interior pathways in Figure 5). In a similar way, the zonal negative gradient in salinity and oxygen concentrations observed between 180° and 140°W at the 2°N stations (EUC-Fe 13 and 1) suggests supplies of fresher northern hemisphere-origin TW (see θ-S plot of TW of EUC-Fe 13, 15, 3 and 1 in Figure 2 and also Figures 5b and 5c), although the lack of ε_{Nd} data in the north does not allow a quantitative estimate. These open ocean lateral supplies of water are consistent with the numerical results obtained by *Grenier et al*. [2011], who discussed the different sources of EUC waters, summarized in their Figure 7. Stations located along the equator (EUC-Fe 14 and 2) seem to be less affected by interior convergent supply, as

suggested by less variable ε_{Nd}, oxygen content and salinity. Interleavings driven by salt fingering observed on the θ-S plots of EUC-Fe 21, 14 and 2 in Figure 2 may rather be formed in the western equatorial Pacific, where LLWBCs converge and imply a mixing of fresh northern TW and salty southern TW [*Fine et al*., 1994; *Kashino et al*., 2007; *Grenier et al*., 2011].

[61] According to *Stramma et al*. [2010], CW and SAMW mix at the equator with water masses originating from the eastern equatorial Pacific OMZ and flowing westward. O_2 and ε_{Nd} data in this study are consistent with this mixing, showing less oxygenated and more radiogenic waters at 140°W than at 156°E, which strongly suggests that the 140°W waters originate from different sources than those at 156°E, as discussed in section 5.2. This hypothesis is also supported by the results of *Grenier et al*., [2011], who showed important recirculation of waters flowing at the interface between the lower EUC and denser westward equatorial currents. In their study, *Stramma et al*. [2010] refer to "westward poorly oxygenated waters". More generally, to our knowledge, these Pacific equatorial 26.8 kg m^{-3} water masses have not been clearly defined yet. We suggest here that these westward-flowing poorly oxygenated waters are modified NPIW. Could NPIW be conveyed partly along the eastern boundaries of the Northern Pacific to the equator and be modified along this pathway, becoming more radiogenic, saltier, and less oxygenated? Our hypothesis is that modified NPIW would be conveyed by the EIC on $\sigma_\theta = 26.8$ kg m^{-3}, as "Eastern Equatorial Pacific Intermediate Water", overlying the EqIW of *Bostock et al*. [2010] because the former is less dense. Confirmation of this hypothesis requires further investigation, both on the NPIW pathway and possible modification and on the tracer characteristics of these waters.

[62] Regarding the IW pathways, new results concerning the deep inter-subtropical circulation reveal the complexity of AAIW flow path from the southern subtropics to the equator. Indeed, *Cravatte et al*. [2012] observed the occurrence of alternated eastward and westward deep zonal jets between 12°S and 12°N, which could even extend further poleward. Our ε_{Nd} and Nd data are too scarce to record the existence of these jets.

[63] As a whole, the complex circulation and potential modification of intermediate and deep waters of the inter-tropical band of the Pacific underline the importance of a better documentation of both its hydrology and geochemistry. The forthcoming GEOTRACES sections GP12 (Pandora Cruise, N/O Atalante, July 2012) and further GP11, GP15, GP19 and GP20 (http://www.geotraces.org) will provide this opportunity.

[64] In the surface waters (SW), *Tazoe et al*. [2011] measured relatively unradiogenic waters ($\varepsilon_{Nd} = -2.7$) at 162°W-, 0° compared to the SW of this study (Figure 4a). Interestingly, both Southern Oscillation Index (SOI) and Oceanic Niño Index (ONI; http://www.cpc.ncep.noaa.gov/products/analysis_monitoring/ensostuff/ensoyears.shtml) indicated La Niña conditions at the time of these author's sampling (ONI = −0.2). In contrast, EUC-Fe cruise occurred during El Niño conditions (ONI = +0.5). These climatic differences support a preferential surfacing of TW (marked by less radiogenic waters) in the central equatorial Pacific during Tazoe and coworkers' sampling, likely explaining the relative unradiogenic values for the SW at that time. This conclusion highlights a particular use of ε_{Nd} as a potentially powerful tracer of vertical processes such as upwelling and downwelling [*Arsouze et al*., 2009].

6. Conclusions

[65] This study investigated the ε_{Nd} and REE concentration evolution of water masses transiting between the subtropics and the equator in the Pacific Ocean.

[66] All the water masses are more radiogenic close to and along the equatorial Pacific than in the subtropics. The release of radiogenic ε_{Nd} by dissolution of continental margin material as water masses flow past is suggested as the main explanation of ε_{Nd} changes observed along the water mass pathways. This hypothesis is supported by the basaltic composition of numerous islands, highly radiogenic for Nd isotopes, located in the inter-tropical Pacific (Figure 12a). The release from dissolution of margin sediments could explain why ε_{Nd} changes occur not only for surface waters but also below the surface and through the entire water column, even for UCDW ($\sigma_\theta = 27.65$ kg m^{-3}; Figure 9a). Many new candidates are added to those previously suggested, the coasts of PNG and New Ireland, as sources of lithogenic ε_{Nd} supply [*Lacan and Jeandel*, 2001], notably (i) coasts of Vanuatu, Fiji, Tonga, and Samoa; (ii) coasts of Gulf of Papua and Solomon Islands; and (iii) Kiribati, Galapagos Islands, and the eastern equatorial coasts of South America (Costa Rica and Ecuador). The Fiji/Tonga ridge and the Pacific mid-oceanic ridge may also contribute to increasing the ε_{Nd} of intermediate and deep water masses. These results underline crucial areas where the ε_{Nd} of water masses is unknown and have to be characterized by further studies (e.g., in the framework of the ongoing GEOTRACES program): between the Tasman Sea and the Coral Sea, upstream and downstream of the Fiji/Tonga ridge, upstream and downstream of Vanuatu, in the Gulf of Papua, and just north of the equator, along the American coasts. Another process that likely impacts the water mass ε_{Nd} is the dissolution of volcanic ashes as they mix with seawater, particularly suggested by the high ε_{Nd} observed for surface waters at stations located northwest of active volcanoes and downwind (stations EUC-Fe 28, 29 and 24).

[67] The relative homogeneity of the averaged isotopic compositions of the sediments and rocks of the inter-tropical Pacific (Figure 12a) highlights the particular necessity to couple the geochemical data with a robust fine-scale description of water mass circulation, in order to avoid misinterpretations of the isotopic variations.

[68] The concentrations of dissolved Nd do not show as clear an evolution as ε_{Nd}, particularly for the water masses flowing below the TW, and are rather marked by relatively constant values (Figure 13). This distribution of Nd concentrations, coupled to ε_{Nd} changes, suggests that boundary exchange, that is, relatively rapid scavenging of material associated with the dissolution of margin sediments [*Lacan and Jeandel*, 2005] is the driving mechanism of the ε_{Nd} evolution in the Pacific Ocean. These results support the hypothesis of *Lacan and Jeandel* [2005] concerning the Nd paradox. However, boundary exchange processes still need to be understood, in order to be correctly parameterized in models.

[69] For each water mass, a positive Eu anomaly characterizes the normalized pattern of dissolved REE. This positive Eu anomaly is also observed for most REE patterns of rocks and sediments collected in the inter-tropical Pacific Ocean (Figure 12b). Thus, consistent with the ε_{Nd} results, the distribution of dissolved REE concentrations and the resulting pattern suggest REE release by dissolution of margin material. The REE patterns and ε_{Nd} evolution together highlight the major role of rock weathering in explaining the distribution of both ε_{Nd} and REE concentrations in the inter-tropical Pacific. In our seawater samples, the Eu anomaly is maintained far from continents that border the Pacific basin, probably because of the abundance of islands and seamounts between the subtropical Pacific and the equator, together with a relatively long Eu residence time (Figure 12a) [*Tomczak and Godfrey*, 2003]. However, the complexity of dissolved/particulate exchange processes is still poorly understood in the geochemical community, and their nature has sparked many debates at recent GEOTRACES meetings. The REE measurement of the particulate fraction will eventually help us, in work to be pursued in the future, to better understand what causes these exchanges, at least in the studied area. Iron (Fe) isotope data may also bring unique insights in that respect, notably about the occurrence (or not) of redox processes associated to those dissolved/particle interactions. Recent iron isotopic data from both dissolved and particulate phases, from samples taken during the EUC-Fe cruise, suggest the occurrence of non-reductive release of dissolved Fe from sediments resuspended from the PNG shelf and slope [*Radic et al*., 2011].

[70] This study also highlights the precision of ε_{Nd} as a tracer of horizontal and vertical mixing occurring between distinct water masses, due to its conservative behavior in the open ocean, far from coasts. Coupled to other parameters such as temperature and salinity, ε_{Nd} contributes to improving our knowledge of the water mass pathways and their variability. However, the scarcity of the data can also lead to misinterpretations and our first estimation of mixing is relatively coarse and cannot take into account numerous different sources. It will be very interesting to verify our suggested conclusions, coupling our Nd results to modeled water mass pathways. These verifications will be investigated in a future study, and water mass transport will be estimated in order to quantify precisely the boundary exchange flux needed to explain the evolution of ε_{Nd} and Nd concentrations.

[71] **Acknowledgments.** The chief scientist of the EUC-Fe cruise, James W. Murray, as well as the captain and the crew of the R/V Kilo Moana are greatly acknowledged. C. Pradoux, J. Rickli, P. Brunet, J. Chmeleff, F. Candaudap, and A. Lanzanova are thanked for their technical support. All the authors whose work contributed to the geological database EarthChem are acknowledged, as well as the EarthChem project office for the availability of the data (http://www.earthchem.org). The authors wish to thank the geochemical team of the SARM (Service d'Analyse des Roches et des Minéraux, CNRS-CRPG, Nancy, France) for the ε_{Nd} and REE concentration measurements of samples of volcano ashes and Bismarck Sea sediments. Conversations with M. Benoit greatly aided the geological interpretation. The authors would like to thank Angélique Melet and Gérard Eldin for the Nd sampling during the FLUSEC cruise, as well as Christophe Maes, chief scientist, for having accepted this additional sampling during the cruise. The authors also want to thank James W. Murray and Luc Beaufort for the gift of sediment samples collected close to PNG coast, in the Bismarck Sea and in the Gulf of Papua, respectively. This work is co-funded by the National Science Foundation (grant NSF-OCE-0425721), by the Agence Nationale de la Recherche (project ANR-09-BLAN-0233-01), and by INSU/LEFE/CYBER project ISOFERIX; it is a contribution to the GEOTRACES and SPICE International programs (http://www.geotraces.org; http://www.solomonseaoceanography.org). Part of this work was supported by COST Action ES0801 "The ocean chemistry of bioactive trace elements and paleoclimate proxies". Finally, we would like to thank Brian Haley and the two anonymous reviewers for their valuable comments and suggestions, which improved the quality of this paper.

References

Alibo, D. S., and Y. Nozaki (1999), Rare earth elements in seawater: Particle association, shale-normalization, and Ce oxidation, *Geochim. Cosmochim. Acta*, *63*(3–4), 363–372. doi:10.1016/S0016-7037(98)00279-8.

Amakawa, H., D. S. Alibo, and Y. Nozaki (2000), Nd isotopic and REE pattern in the surface waters of the eastern Indian Ocean and its adjacent seas, *Geochim. Cosmochim. Acta*, *64*, 1715–1727.

Aplin A., A. Michard, and F. Albarede (1986/1987), $^{143}Nd/^{144}Nd$ in Pacific ferromanganese encrustations and nodules, *Earth Planet. Sci. Lett.*, *81*, 7–14.

Akagi, T., F. Fu, Y. Hongo, and K. Takahashi (2011), Composition of rare earth elements in settling particles collected in the highly productive North Pacific Ocean and Bering Sea: Implications for siliceous-matter dissolution kinetics and formation of two REE-enriched phases, *Geochim. Cosmochim. Acta*, *75*, 4857–4876.

Arsouze, T., J.-C. Dutay, F. Lacan, C. Jeandel (2009), Reconstructing the Nd oceanic cycle using a coupled dynamical–biogeochemical model, *Biogeosciences*, *6*(12), 2829–2846. doi:10.5194/bg-6-2829-2009.

Bertram, C. J., and H. Elderfield (1993), The geochemical balance of the rare earth elements and Nd isotopes in the oceans, *Geochim. Cosmochim. Acta*, *57*, 1957–1986.

Bingham, F. M., and R. Lukas (1994), The southward intrusion of North Pacific Intermediate Water along the Mindanao coast, *J. Phys. Oceanogr.*, *24*, 141–154.

Bostock, H. C., B. N. Opdyke, and M. J. M. Williams (2010), Characterising the intermediate depth waters of the Pacific Ocean using $\delta^{13}C$ and other geochemical tracers, *Deep Sea Res.*, *57*, 847–859. doi:10.1016/j.dsr.2010.04.005.

Byrne, R. H., and K.-H. Kim (1990), Rare earth element scavenging in seawater, *Geochim. Cosmochim. Acta*, *54*, 2645–2656.

Byrne, R. H., and K.-H. Kim (1993), Rare earth precipitation and coprecipitation behavior: The limiting role of PO_4^{3-} on dissolved rare earth concentrations in seawater, *Geochim. Cosmochim. Acta*, *57*, 519–526.

Byrne, R. H., and E. R. Sholkovitz (1996), Marine chemistry and geochemistry of the lanthanides, in *Handbook on the Physics and Chemistry of Rare Earths*, Elsevier Sci., New York, pp. 527–537.

Callahan, J. E. (1972), The structure and circulation of deep water in the Antarctic, *Deep Sea Res.*, *19*, 563–575.

Carignan J., P. Hild, G. Mevelle, J. Morel, and D. Yeghicheyan (2001), Routine analyses of trace elements in geological samples using flow injection and low pressure on-line liquid chromatography coupled to ICP-MS: A study of geochemical reference materials BR, DR-N, AN-G and GH, *Geostand. Newsl.*, *25*, 187–198.

Carter, P., D. Vance, C. D. Hillenbrand, J. A. Smith, and D. R. Shoosmith (2012), The neodymium isotopic composition of waters masses in the eastern Pacific sector of the Southern Ocean, *Geochim. Cosmochim. Acta*, *79*, 41–59.

Chung, C.-H., I. Brenner, C.-F. You (2009), Comparison of microconcentric and membrane-desolvation sample introduction systems for determination of low rare earth element concentrations in surface and subsurface waters using sector field inductively coupled plasma mass spectrometry, *Spectrochim. Acta B*, *64*, 849–856.

Coale, K. H., S. E. Fitzwater, R. M. Gordon, K. S. Johnson, and R. T. Barber (1996), Control of community growth and export production by upwelled iron in the equatorial Pacific Ocean, *Nature*, *379*, 621–624.

Craddock P. R., W. Bach, J. S. Seewald, O. J. Rouxel, E. Reeves, and M. K. Tivey (2010), Rare earth element abundances in hydrothermal fluids from the Manus Basin, Papua New Guinea: Indicators of sub-seafloor hydrothermal processes in back-arc basins, *Geochim. Cosmochim. Acta*, *74*, 5494–5513.

Cravatte, S., A. Ganachaud, Q.-P. Duong, W. S. Kessler, G. Eldin, and P. Dutrieux (2011), Observed circulation in the Solomon Sea from SADCP data, *Prog. Oceanogr.*, *88*, 116–130, doi:10.1016/j.pocean.2010.12.015.

Cravatte, S., W. S. Kessler, and F. Marin (2012), Intermediate zonal jets in the Tropical Pacific Ocean observed by Argo floats, *J. Phys. Oceanogr.*, *42*, 1475–1485, doi:10.1175/JPO-D-11-0206.1.

De Baar, H. J. W., M. P. Bacon, P. G. Brewer, K. W. Bruland (1985), Rare-earth elements in the Pacific and in the Atlantic Oceans, *Geochim. Cosmochim. Acta*, *49*, 1953–1959.

Elderfield, H., and M. J. Greaves (1982), The rare earth elements in seawater, *Nature*, *296*, 214–219.

Elderfield, H. (1988), The oceanic chemistry of the rare earth elements, *Philos. Trans. R. Soc. Ser. A.*, *325*, 105–126.

Fine, R. A., R. Lukas, F. Bingham, M. J. Warnar, and R. H. Gammon (1994), The western equatorial Pacific: A water mass crossroads, *J. Geophys. Res.*, *99*, 25 063–25 080.

Firing, E., S. E. Wijffels, and P. Hacker (1998), Equatorial subthermocline currents across the Pacific, *J. Geophys. Res.*, *103*, 21413–21423.

Fukumori, I., T. Lee, B. Cheng, and D. Menemenlis (2004), The origin, pathway, and destination of Niño-3 water estimated by a simulated passive tracer and its adjoint, *J. Phys. Oceanogr.*, *34*, 582–604.

Gasparin, F., A. Ganachaud, and C. Maes (2011), A western boundary current east of New Caledonia: Observed characteristics, *Deep Sea Res. I*, *58*, 956–969.

Gasparin F., A. Ganachaud, C. Maes, F. Marin, and G. Eldin (2012), Oceanic transports through the Solomon Sea: The bend of the New Guinea Coastal Undercurrent, *Geophys. Res. Lett.*, *39*, L15608, doi:10.1029/2012GL052575.

German, C. R., G. P. Klinkhammer, J. M. Edmond, A. Mitra, and H. Elderfield (1990), Hydrothermal scavenging of rare earth elements in the ocean, *Nature*, *345*, 516–518.

Goldstein, S., and S. R. Hemming (2003), Long Lived Isotopic Tracers in Oceanography, Paleoceanography and Ice-sheet Dynamics. Treatise on Geochemistry, ch 6.17, vol. *6*. Elsevier, New York, pp. 453–489.

Grasse, P., T. Stichel, R. Stumpf, L. Stramma, and M. Frank (2012), The distribution of neodymium isotopes and concentrations in the eastern equatorial Pacific: Water mass advection versus particle exchange, *Earth Planet. Sci. Lett.*, *353–354*, 198–207, doi:http://dx.doi.org/10.1016/j.epsl.2012.07.044.

Grenier, M., S. Cravatte, B. Blanke, C. Menkes, A. Koch-Larrouy, F. Durand, A. Melet, and C. Jeandel (2011), From the western boundary currents to the Pacific Equatorial Undercurrent: Modeled pathways and water mass evolutions, *J. Geophys. Res.*, *116*, C12044, doi:10.1029/2011JC007477.

Hannigan, R., and E. Sholkovitz (2001), The development of middle rare earth element enrichments in freshwaters: weathering of phosphate minerals, *Chem. Geol.*, *175*(3–4), 495–508.

Hristrova, H. G., and W. S. Kessler (2012), Surface circulation in the Solomon Sea derived from Lagrangian drifter observations, *J. Phys. Oceanogr.*, *42*, 448–458. doi:10.1175/JPO-D-11-099.1.

Horikawa, K., E. E. Martin, Y. Asahara, and T. Sagawa (2011), Limits on conservative behavior of Nd isotopes in seawater assessed from analysis of fish teeth from Pacific core tops, *Earth Planet. Sci. Lett.*, *310*, 119–130.

Jeandel, C., J. K. Bishop, and A. Zindler (1995), Exchange of Nd and its isotopes between seawater small and large particles in the Sargasso Sea, *Geochim. Cosmochim. Acta*, *59*, 535–547.

Jeandel C., T. Arsouze, F. Lacan, P. Techine, and J.-C. Dutay (2007), Isotopic Nd compositions and concentrations of the lithogenic inputs into the ocean: A compilation, with an emphasis on the margins, *Chem. Geol.*, *239*, 156–164. doi:10.1016/j.chemgeo.2006.11.013.

Jeandel, C., B. Peucker-Ehrenbrink, M. T. Jones, C. R. Pearce, E. H. Oelkers, Y. Godderis, F. Lacan, O. Aumont, and T. Arsouze (2011), Ocean margins: The missing term for oceanic element budgets? *Eos Trans. AGU*, *92*(26), 217–219.

Jeandel, C., H. Delattre, M. Grenier, C. Pradoux, and F. Lacan (2013), Rare earth element concentrations and Nd isotopes in the South East Pacific Ocean, *Geochem. Geophys. Geosyst.*, doi:10.1029/2012GC004309, in press.

Johnson, G. C., and M. J. McPhaden (1999), Interior pycnocline flow from the subtropical to the equatorial Pacific Ocean, *J. Phys. Oceanogr.*, *29*, 3073–3089.

Johnson, G. C. (2001), The Pacific Ocean subtropical cell surface limb, *Geophy. Res. Lett.*, *28*(9), 1771–1774, doi:10.1029/2000GL012723.

Kashino, Y., I. Ueki, Y. Kuroda, and A. Purwandani (2007), Ocean variability north of New Guinea derived from TRITON buoy data, *J. Oceanogr.*, *63*(4), 545–559.

Kawabe, M., and S. Fujio (2010), Pacific Ocean circulation based on observation, *J. Oceanogr.*, *66*, 389–403.

Kineke, G. C., K. J. Woolfe, S. A. Huehl, J. D. Milliman, T. M. Dellapenna, and R. G. Purdon (2000), Sediment export from the Sepik River, Papua New Guinea: Evidence for a divergent sediment plume, *Cont. Shelf Res.*, *20*, 2239–2266.

Konter, J. G., B. B. Hanan, J. Blichert-Toft, A. A. P. Koppers, T. Plank, and H. Staudigel (2008), One hundred million years of mantle geochemical history suggest the retiring of mantle plumes is premature, *Earth Planet. Sci. Lett.*, *275*, 285–295, doi:10.1016/j.epsl.2008.08.023.

Lacan, F., and C. Jeandel (2001), Tracing Papua New Guinea imprint on the central equatorial Pacific Ocean using neodymium isotopic compositions and rare earth element patterns, *Earth Planet. Sci. Lett.*, *186*, 497–512, doi:10.1016/S0012-821X(01)00263-1.

Lacan, F., and C. Jeandel (2005), Neodymium isotopes as a new tool for quantifying exchange fluxes at the continent–ocean interface, *Earth Planet. Sci. Lett.*, *232*(3–4), 245–257. doi:10.1016/j.epsl.2005.01.004.

Lacan, F., K. Tachikawa, and C. Jeandel (2012), Neodymium isotopic composition of the oceans: A compilation of seawater data, *Chem. Geol.*, *300-301*, 177–184. doi:10.1016/j.chemgeo.2012.01.019.

Lagerloef, G. S. E., G. T. Mitchurn, R. B. Lukas, and P. P. Niiler (1999), Tropical Pacific near-surface currents estimated from altimeter, wind, and drifter data, *J. Geophys. Res.*, *104*, 23,313–23,326.

Lee, J. H., and R. H. Byrne (1993), Complexation of trivalent rare earth elements (Ce, Eu, Gd, Tb, Yb) by carbonate ions, *Geochim. Cosmochim. Acta*, *57*, 295–302.

Mackey, D. J., J. E. O'Sullivan, and R. J. Watson (2002), Iron in the western Pacific: A riverine or hydrothermal source for iron in the Equatorial Undercurrent, *Deep Sea Res.*, Part I, *49*, 877–893.

Maes, C., G. Eldin, A. Melet, J. Lefévre, J. Sudre, D. Varillon, A. Ganachaud, and L. Gourdeau (2009), Rapport de la mission océanographique FLUSEC-01 à bord du N. O. Alis du 12 au 30 Août 2007 en mer de Corail, Océan Pacifique Sud-Ouest, Rapports de missions, Sciences de la Mer, Océanographie Physique, Centre IRD de Nouméa, Nouvelle Calédonie, No. 24, 98 pp.

Marin, F., E. Kestenare, T. Delcroix, F. Durand, S. Cravatte, G. Eldin, and R. Bourdallé-Badie (2010), Annual reversal of the EIC in the Pacific: Observations and model diagnostics, *J. Phys. Oceanogr.*, *40*, 915–933, doi:10.1175/2009JPO4318.1.

McCartney, M. S. (1977), Subantarctic mode water, *Deep Sea Res.*, *24*, 103–119.

McLennan, S. M. (1989), Rare earth elements in sedimentary rocks: influence of provenance and sedimentary processes in *Geochemistry and Mineralogy of Rare Earth Elements* edited by B. R. Lipin and G. H. Mckay, Reviews in Mineralogy, vol. 21, 169–200, Mineralogical Society of America, Washington, D.C.

Messié, M., M.-H. Radenac, J. Lefèvre, P. Marchesiello (2006), Chlorophyll bloom in the western Pacific at the end of the 1997–1998 El-Nino: The role of the Kiribati Islands, *Geophys. Res. Lett.*, *33*, L14601, doi:10.1029/2006GL026033.

Michard, A., F. Albarède, G. Michard, J. F. Minster, and J. L. Charlou (1983), Rare-earth elements and uranium in high-temperature solutions from East Pacific Rise hydrothermal vent field (13°N), *Nature*, *303*, 795–797.

Nozaki, Y., and D. S. Alibo (2003a), Importance of vertical geochemical processes in controlling the oceanic profiles of dissolved rare earth elements in the northeastern Indian Ocean, *Earth Planet. Sci. Lett.*, *205*, 155–172.

Nozaki, Y., and D. S. Alibo (2003b), Dissolved rare earth elements in the Southern Ocean, southwest of Australia: Unique patterns compared to the South Atlantic data, *Geochem. J.*, *37*, 47–62.

Nozaki, Y., D. S. Alibo, H. Amakawa, T. Gamo, and H. Hasumoto (1999), Dissolved rare earth elements and hydrography in the Sulu Sea, *Geochim. Cosmochim. Acta*, *63*, 2171–2181.

Olivarez, A. M., and R. M. Owen (1989), REE/Fe variation in hydrothermal sediments: Implication for the REE content of seawater, *Geochim. Cosmochim. Acta*, *53*, 757-762.

Orsi, A. H., T. Whitworth III, and W. D. Nowlin Jr. (1995), On the meridional extent and fronts of the Antarctic circumpolar current, *Deep Sea Res. I*, *42*, 641–673.

Orsi, A. H., G. C. Johnson, and J. L. Bullister (1999), Circulation, mixing and production of Antarctic Bottom Water, *Prog. Oceanogr.*, *43*, 55–109.

Pahnke, K., T. van de Flierdt, K. M. Jones, M. Lambelet, S. R. Hemming, and S. L. Goldstein (2012), GEOTRACES intercalibration of neodymium isotopes and rare earth element concentrations in seawater and suspended particles—Part 2: Systematic test and baseline profiles, *Limnol. Oceanogr.*, *10*, 252–269, doi: 10.4319/lom.2012.10.252.

Piepgras, D. J., and G. J. Wasserburg (1982), Isotopic composition of neodymium in waters from the Drake Passage, *Science*, *217*, 207–217.

Piepgras, D. J., and S. B. Jacobsen (1992), The behavior of rare earth elements in seawater: Precise determination of variation in the North Pacific water column, *Geochim. Cosmochim. Acta*, *56*, 1851–1862, doi:10.1016/0016-7037(92)90315-A.

Pin, C., and J. F. S. Zalduegui (1997), Sequential separation of light rare-earth elements, thorium and uranium by miniaturized extraction chromatography: Application to isotopic analyses of silicate rocks, *Anal. Chim. Acta*, *339*, 79– 89.

Qu, T., and E. J. Lindstrom (2002), A climatological interpretation of the circulation in the Western South Pacific, *J. Phys. Oceanogr.*, *32*(9), 2492–2508.

Qu, T., and E. J. Lindstrom (2004), Northward intrusion of Antarctic Intermediate Water in the western Pacific, *J. Phys. Oceanogr.*, *34*, 2104–2118.

Qu, T., S. Gao, I. Fukumori, R. Fine, and E. J. Lindstrom (2009), Origin and pathway of equatorial 13°C water in the Pacific identified by a simulated passive tracer and its adjoint, *J. Phys. Oceanogr.*, *39*, 1836–1853.

Radic, A., F. Lacan, and J. W. Murray (2011), Isotopic composition of dissolved iron in the equatorial Pacific Ocean: New constraints for the oceanic iron cycle, *Earth Planet. Sci. Lett.*, *306*, 1–10. doi:10.1016/j.epsl.2011.03.015.

Reid, J. L. (1997), On the total geostrophic circulation of the Pacific Ocean: Flow patterns, tracers, and transports, *Prog. Oceanogr.*, *39*, 263–352.

Reverdin, G., C. Frankignoul, E. Kestenare, and M. McPhaden (1994), Seasonal variability on the surface currents of the equatorial Pacific, *J. Geophys. Res.*, *99*, 20,323–20,344.

Rickli, J. D., M. Frank, A. R. Backer, S. Aciego, G. de Souza, R. B. Georg, and A. N. Halliday (2010), Hafnium and neodymium isotopes in surface waters of the eastern Atlantic Ocean: Implications for sources and inputs of trace metals to the ocean, *Geochim. Cosmochim. Acta*, *74*, 540–557, doi:10.1016/j.gca.2009.10.006.

Rowe, G. D., E. Firing, and G. C. Johnson (2000), Pacific equatorial subsurface countercurrent velocity, transport, and potential vorticity, *J. Phys. Oceanogr.*, *30*, 1172–1187.

Ryan, J. P., I. Ueki, Y. Chao, H. Hang, P. S. Polito, and F. P. Chavez (2006), Western Pacific modulation of large phytoplankton blooms in the central and eastern equatorial Pacific, *J. Geophys. Res.*, *111*, G02013, doi:10.1029/2005JG000084.

Shabani, M. B., T. Akagi, and A. Masuda (1992), Preconcentration of trace rare-earth elements in seawater by complexation with bis(2-ethylhexyl) hydrogen phosphate and 2-ethylhexyl dihydrogen phosphate adsorbed on a C_{18} cartridge and determination by inductively coupled plasma mass spectrometry, *Anal. Chem.*, *64*, 737–743.

Sholkovitz, E. R., W. M. Landing, and B. L. Lewis (1994), Ocean particle chemistry: The fractionation of rare earth elements between suspended particles and seawater, *Geochim. Cosmochim. Acta*, *58*, 1567–1579.

Sholkovitz, E. R., H. Elderfield, R. Szymczak, and K. Casey (1999), Island weathering: River sources of rare earth elements to the Western Pacific Ocean, *Mar. Chem.*, *68*, 39–57.

Sholkovitz, E., and R. Szymczak (2000), The estuarine chemistry of rare earth elements: Comparison of the Amazon, Fly, Sepik and the Gulf of Papua system, *Earth Planet. Sci. Lett.*, *179*, 299–309.

Slemons, L. O., J. W. Murray, T. Gorgues, O. Aumont, and C. Menkes (2009), Biogeochemical impact of a model western iron source in the Pacific Equatorial Undercurrent, *Deep Sea Res.*, Part I, doi:10.1016/j.dsr.2009.08.005.

Slemons, L. O., J. W. Murray, B. Paul, and P. Dutrieux (2010), Western Pacific coastal sources of iron, manganese and aluminium to the Equatorial Undercurrent, *Global Biogeochem. Cy.*, *24*, GB3024, doi:10.1029/2009 GB003693.

Sokolov, S., and S. Rintoul (2000), Circulation and water masses of the south west Pacific: WOCE section P11, Papua New Guinea to Tasmania, *J. Mar. Res.*, *58*, 223–268.

Stramma, L., G. C. Johnson, E. Firing, and S. Schmidtko (2010), Eastern Pacific oxygen minimum zones: Supply paths and multidecadal changes, *J. Geophys. Res.*, *115*, C09011, doi:10.1029/2009JC005976.

Sun, S.-S., and W. F. McDonough (1989), Chemical and isotopic systematics of oceanic basalts: Implications for mantle composition and processes, in *Magmatism in the Ocean Basins*, A. D. Saunders, and M. J. Norry, *Geological Society of London*, London, *42*, 313–345.

Tachikawa, K., C. Jeandel, and M. Roy-Barman (1999), A new approach to Nd residence time in the ocean: The role of atmospheric inputs, *Earth Planet. Sci. Lett.*, *170*, 433–446.

Tachikawa, K., V. Athias, and C. Jeandel (2003), Neodymium budget in the ocean and paleoceanographic implications, *J. Geophys. Res.*, *108*, 3254, doi:10.1029/1999JC000285.

Takebe, M. (2005), Carriers of rare earth elements in Pacific deep-sea sediments, *J. Geol.*, *113*, 201–215.

Talley, L. D. (1993), Distribution and formation of North Pacific Intermediate Water, *J. Phys. Oceanogr.*, *23*, 517–537.

Tazoe, H., H. Obata, and T. Gamo (2011), Coupled isotopic systematics of surface cerium and neodymium in the Pacific Ocean, *Geochem. Geophy. Geosy.*, *12*, Q04004, doi:10.1029/2010GC003342.

Tomczak, M., and D. Hao (1989), Water masses in the thermocline of the Coral Sea, *Deep Sea Res.*, *36*(10), 1503–1514.

Tomczak, M., and J. S., Godfrey (2003), Hydrology of the Pacific Ocean, Regional Oceanography: An Introduction, 2nd Improved Edition. Daya Publishing House, Delhi, pp. 137–156.

Tsimplis, M., S. Bacon, and H. L. Bryden (1998), The circulation of the subtropical south Pacific derived from hydrographic data, *J. Geophys. Res.*, *103*, 21443–21468.

Tsuchiya, M. (1981), The origin of the Pacific equatorial 13°C water, *J. Phys. Oceanogr.*, *11*, 794–812.

Tsuchiya, M. (1991), Flow path of the Antarctic Intermediate Water in the western equatorial South Pacific Ocean, *Deep Sea Res.*, *38*(Suppl. l), S273–S279.

Tsuchiya, M., and L. D. Talley (1996), Water property distributions along an eastern Pacific hydrographic section at 135W, *J. Mar. Res.*, *54*, 541–564.

Tsuchiya, M., and L. D. Talley (1998), A Pacific hydrographic section at 88°W: Water property distribution, *J. Geophys. Res.*, *103*, 12899–12918.

Tsuchiya, M., R. Lukas, R. Fine, E. Firing, and E. Lindstrom (1989), Source waters of the Pacific Equatorial Undercurrent, *Prog. Oceanogr.*, *23*, 101–147.

Ueki, I., Y. Kashino, and Y. Kuroda (2003), Observation of current variations off the New Guinea coast including the 1997–1998 El Niño period and their relationship with Sverdrup transport, *J. Geophys. Res.*, *108*(C7).

van de Flierdt, T., K. Pahnke, and GEOTRACES intercalibration participants (2012), GEOTRACES intercalibration of neodymium isotopes and rare earth element concentrations in seawater and suspended particulates—Part 1: International intercomparison, *Limnol. and Oceanogr.*, *10*, 234–251, doi:10.4319/lom.2012.10.234.

Vance, D., and M. F. Thirlwall (2002), An assessment of mass discrimination in MC-ICPMS using Nd isotopes, *Chem. Geol.*, *185*, 227–240.

Wang, Z.-L., and M. Yamada (2007), Geochemistry of dissolved rare earth elements in the Equatorial Pacific Ocean, *Environ. Geol.*, *52*, 779–787.

Wasserburg, G. J., S. B. Jacobsen, D. L. De Paolo, M. T. McCulloch, and T. Wen (1981), Precise determination of Sm/Nd ratios, Sm and Nd isotopic abundances in standard solutions, *Geochim. Cosmochim. Acta*, *45*, 2311–2323.

Wyrtki, K. (1962), The subsurface water masses in the western South Pacific Ocean, *Aust. J. Mar. Freshwater Res.*, *13*, 18–47.

You, Y. (2003), The pathway and circulation of North Pacific Intermediate Water, *Geophys. Res. Lett.*, *30*(24), 2291, doi:10.1029/2003GL018561.

You, Y., N. Suginohara, M. Fukasawa, H. Yoritaka, K. Mizuno, Y. Kashino, and D. Hartoyo (2003), Transport of North Pacific Intermediate Water across Japanese WOCE sections, *J. Geophys. Res.*, *108*(C6), 3196, doi:10.1029/2002JC001662.

Zenk, W., G. Siedler, A. Ishida, J. Holfort, Y. Kashino, Y. Kuroda, T. Miyama, and T. J. Müller (2005), Pathways and variability of the Antarctic Intermediate Water in the western equatorial Pacific Ocean, *Prog. Oceanogr.*, *67*, 245–281.

Zhang, J., and Y. Nozaki (1996), Rare earth elements and yttrium in seawater: ICP-MS determinations in the East Caroline, Coral Sea and South Fiji basins of the western south Pacific Ocean, *Geochim. Cosmochim. Acta*, *60*, 4631– 4644.

Zhang, Y., F. Lacan, and C. Jeandel (2008), Dissolved rare earth elements tracing lithogenic inputs over the Kerguelen plateau (Southern Ocean), *Deep Sea Res. II*, *55*(5–7), 638–652, doi:10.1016/j.dsr2.2007.12.029.